

# Task-parallelism in SWIFT for heterogeneous compute architectures

Abouzied M. A. Nasar<sup>1\*</sup>, Benedict D. Rogers<sup>1</sup>, Georgios Fourtakas<sup>1</sup>, Scott T. Kay<sup>2</sup> and Matthieu Schaller<sup>3,4</sup>.

<sup>1</sup>*School of Engineering, The University of Manchester, Nancy Rothwell Building, Manchester M13 9QS, UK.*

<sup>2</sup>*Department of Physics and Astronomy, The University of Manchester, Schuster Building, Manchester, M139PL, UK.*

<sup>3</sup>*Lorentz Institute for theoretical physics, Leiden University, PO Box 9506, NL-2300 RA, Leiden, The Netherlands.*

<sup>4</sup>*Leiden observatory, Leiden University, PO Box 9513, NL-2300 RA, Leiden, The Netherlands.*

## ABSTRACT

This paper highlights the first steps towards enabling graphics processing unit (GPU) acceleration of the smoothed particle hydrodynamics (SPH) solver for cosmology SWIFT and creating a hydrodynamics solver capable of fully leveraging the hardware available on heterogeneous exascale machines composed of central and graphics processing units (CPUs and GPUs). Exploiting the existing task-based parallelism in SWIFT, novel combinations of algorithms are presented which enable SWIFT to function as a truly heterogeneous software leveraging CPUs for memory-bound computations concurrently with GPUs for compute-bound computations in a manner which minimises the effects of CPU-GPU communication latency. These algorithms are validated in extensive testing which shows that the GPU acceleration methodology is capable of delivering up to  $\sim 3.5x$  speedups for SWIFT's SPH hydrodynamics computation kernels when including the time required to prepare the computations on the CPU and unpack the results on the CPU. Speedups of  $\sim 7.5x$  are demonstrated when not including the CPU data preparation and unpacking times. Whilst these measured speedups are substantial, it is shown that the overall performance of the hydrodynamic solver for a full simulation when accelerated on the GPU of state-of-the-art superchips, is only marginally faster than the code performance when using the Grace Hopper superchip's fully parallelised CPU capabilities. This is shown to be mostly due to excessive fine-graining of the tasks prior to offloading on the GPU. Fine-graining introduces significant over-heads associated with task management on the CPU hosting the simulation and also introduces un-necessary duplication of CPU-GPU communications of the same data.

**Key words:** GPU acceleration – High-performance computing – Smoothed Particle Hydrodynamics – Software – Algorithms

## 1 INTRODUCTION

Numerical Astrophysics simulations are a unique tool in cosmology as they allow a deeper understanding of galaxy evolution (Vogelsberger et al., 2020), planetary collisions (Kegerreis et al., 2019) and other complex phenomena (Andrade et al., 2022), that would not be possible using observations. Given the complexity of physical processes included, the range of density and timescale variations and the fact that most of the universe is empty space, cosmology solvers typically rely on Lagrangian methods such as smoothed particle hydrodynamics (SPH) (Hopkins, 2017; Wadsley, Keller & Quinn, 2017; Price et al., 2018) and moving mesh methods (Springel, 2010; Chang, Wadsley & Quinn, 2017). These Lagrangian methods can handle the complex physics and are also able to capture rapidly deforming pockets of matter. Eulerian mesh-based solvers also exist such as Athena++ (Stone et al., 2020), PLUTO (Mignone et al., 2011) and RAMSES (Teyssier, 2002) which rely on more complex adaptive mesh-refinement (AMR) techniques to dynamically adapt the mesh to the

physics to ensure high resolution is only used where required for computational efficiency.

The scale of astrophysics simulations has been increasing rapidly and recently deployed high-fidelity digital twins of the universe, (Pakmor et al., 2023) and (Schaye et al., 2023) for example, are allowing researchers to better understand the complexities of the tightly coupled non-linear physics which govern the Universe's behaviour. Simulations at this scale require massive resolution with  $O(10^{10}$  to  $10^{11})$  computational points in order to resolve the complex physics accurately. Such large simulations must be run on supercomputers using codes designed to maximise computational weak scalability. These models are highly efficient, however to account for unresolved physics sub-grid modelling is a necessity given the large scale variations in the physics governing the Universe (Crain & van de Voort, 2023). The model's overall accuracy and the accuracy of these sub-grid models (Vogelsberger et al., 2020) is dependent on the resolution used for the simulations and as such there is still a pressing need for higher fidelity simulations

using more computational nodes to discretise the universe. Given the recent advances in supercomputers where the ExaFLOP barrier has been broken (Atchley et al., 2023), it could be argued that a step-change in our ability to resolve astrophysical phenomena using simulations is now within reach if the argument was purely based on the increase in computational power available. However, the architecture of new exascale supercomputers which are benchmarked achieving  $10^{18}$  floating point operations per second (FLOPS) is dominated by heterogeneous architectures employing graphics processing unit (GPU) acceleration. Hence, existing astrophysics solvers previously designed for massively parallel CPU execution must be adapted to benefit from GPU acceleration.

Partly due to the boom in artificial intelligence (AI) and machine learning (ML), specialised HPC superchips have been developed such as Nvidia's Grace-Hopper (Schieffer et al., 2024) and AMD's MI300x (Smith et al., 2024) which are set to feature heavily in new supercomputer architectures (Herten et al., 2024; McIntosh-Smith, Alam & Woods, 2024; Fusco et al., 2024; Herten, 2023). These superchips offer large CPU memory (480 GB for the Grace CPU in the Grace-Hopper chip) complementing relatively smaller GPU memory (96 GB for its Hopper GPU) with CPU-GPU memory cache-coherency *and* a superfast CPU-GPU connection to allow for:

- a- Usage of larger data sets than possible with the conventional general-purpose GPU (GPGPU) computer architectures.
- b- Minimal loss in GPU acceleration efficiency due to slow CPU-GPU data transfers.

The importance of the CPU-GPU connection speed is widely recognised in the HPC community as typically, CPU-GPU communications over conventional PCIe ports tend to be the first bottleneck encountered in many applications (Pabst, Koch & Straßer, 2010; Xu, Jeon & Annavaram, 2014). This importance is evidenced at the time of writing by two of the world's leading supercomputers, Summit and Frontier, using AMD's Infinity Fabric and Nvidia's NVLink connections to deliver greater bandwidth, 72 GB/s (Pearson, 2023) and 50 GB/s (Vergara Larrea et al., 2019) respectively, than via PCIe ports of the same generation (PCIe 4 and PCIe 3 with 32 GB/s and 16 GB/s, respectively)..

Computational fluid dynamics (CFD) generally requires HPC for accurate flow simulation especially when attempting to accurately capture complex phenomena such as turbulence (López et al., 2020), combustion (Kolla & Chen, 2017) and multi-phase flow (Karnakov et al., 2019). As such, development of general purpose CFD solvers capable of efficiently leveraging Exascale architectures (especially current machines which are heterogeneous) is a very active field of research. An extremely wide variety of approaches to developing exascalable CFD solvers have been proposed using different techniques such as finite volume methods (Sharma et al., 2024; Antoniadis et al., 2022), mixed finite volume finite element methods (Gorobets & Bakhvalov, 2022), spectral element methods (Merzari et al., 2024; Lindblad et al., 2023), finite difference methods (Deskos, Laizet & Palacios, 2020) and of course SPH (Guerrera et al., 2019). A methodology highly relevant to the research presented in this paper is the approach used by the UinTAH solver (Holmen, Sahasrabudhe & Berzins, 2022) which also uses a tasking approach to distribute the workload between the available computational hardware. UinTAH uses task schedulers to execute tasks simultaneously across the available hardware (CPUs and GPUs) based upon user-specification of which hardware to use for running different task types. This is similar to the approach we propose in this paper where we use a custom purpose-built task scheduler, QuickSched (Gonnet, Chalk & Schaller, 2016), similar in function to the task scheduler within the UinTAH solver framework (Holmen, Sahasrabudhe & Berzins, 2022). However, in UinTAH the scheduler is designed to maximise code portability where it also acts as an abstraction layer for several different computational modules solving different physics and uses the highly portable Kokkos framework (Edwards, Trott & Sunderland, 2014) to schedule computations for execution on the available hardware (CPUs and GPUs) according to the user's specifications.

SPH with inter-dependent fine-grained tasking (SWIFT<sup>1</sup>) (Schaller et al., 2024) is an open-source Astrophysics solver which uses task-parallelism instead of conventional data-parallelism to maximise the solver's scalability especially for complex simulations involving large scale disparity which require extreme spatial *and* temporal adaptivity (Borrow et al., 2018). SWIFT relies on a custom task scheduler QuickSched (Gonnet, Chalk & Schaller,

---

<sup>1</sup> <https://swift.strw.leidenuniv.nl/>

2016) which re-defines all the computations and communications required for a simulation as small fine-grained tasks which can be executed by any of the available computational threads as and when their dependencies (completion of other tasks) have been fulfilled. This approach minimises idle time due to load imbalance and in principle allows for MPI communications to be inter-leaved with computations such that data transfers in between MPI ranks are hidden underneath computations. Whilst SWIFT scales exceptionally well on CPUs (with only 15% loss in performance when weak scaling from one compute node with 128 CPU cores to 343 compute nodes with more than 40k CPU cores) (Schaller et al., 2024), GPU acceleration of the solver such that task management is also performed by the GPU is a difficult endeavour as the memory access intensive task management process does not easily lend itself to GPU acceleration. GPUs are extremely efficient for computations where all the available hardware threads are performing the same computation on different portions of the same data as this minimises kernel launch overheads and optimises memory access (Cook, 2012). SWIFT's task manager however requires random access to many different small packets of data for the management of the different task types which typically occur concurrently and as such GPU acceleration is difficult (Chalk & Bernard, 2017).

The conventional approach to GPGPU acceleration for SPH (Domínguez et al., 2022; Bilotta et al., 2016; Cercos-Pita, 2015) has been such that data is designed to reside on GPUs for the entire simulation as this allows the data to be re-used for all computations eliminating losses in efficiency induced by a von Neumann-esque bottleneck (CPU-GPU communication overheads). This approach is especially advantageous for pre-exascale architectures where the GPU is connected to the compute node via a relatively slow PCIe port. Massive gains in performance have been demonstrated by DualSPHysics (Domínguez et al., 2022), GPUSPH (Bilotta et al., 2016), SHAMROCK (David-Cléris, Laibe & Lapeyre, 2025) and SPH-EXA (Sanz Lechuga, 2022) which were designed for such architectures. New pre-exascale machines however, such as the European supercomputer Jupiter (Herten et al., 2024) and the UK based Isambard-AI (McIntosh-Smith, Alam & Woods, 2024) for example, leverage superchips composed of GPUs *and* high-powered CPUs connected via a purpose-built connection, up to 7x faster than current PCIe 5 ports, such that the much larger CPU memory (480 GB CPU memory vs 96 GB GPU memory for

the GH200 superchip (Fusco et al., 2024)) can be leveraged to increase problem size dramatically without a significant loss in performance. As these new Exascale machines were designed specifically to overcome the limitations associated with the smaller GPU memory, deployment of simulations using the conventional approach to GPU acceleration of SPH would leave a great deal of the machine's resources untapped.

Parallelisation of SPH on single compute nodes using shared memory parallelisation strategies with OpenMP or TBB for example is relatively straightforward and has been applied effectively in many SPH solvers for engineering and other terrestrial applications ((Ramachandran et al., 2021; Zhang et al., 2021) for example). However, the scale of Astrophysics and cosmology applications requires extreme parallelisation on thousands of compute nodes and as such, advanced extremely scalable techniques for distributed memory parallelisation are required. These strategies must overcome a number of obstacles. The Lagrangian nature of the method which leads to the computational points (particles) leaving and entering different parts of the distributed memory (requiring robust domain decomposition strategies (Guo et al., 2018)), Temporal adaptivity (as required for feasible time-to-solution where particles have different time step sizes depending on their size and other factors related to CFL conditions) can also have a strong influence on the computational work available to each node at a given point in the simulation (Borrow et al., 2018) as it is difficult to decompose the domain in between compute nodes to ensure each node has a similar number of particles with similar time step sizes. In cases involving gravitational forces particles cluster in regions of the domain which again complicates load balancing and domain decomposition and techniques such as tree based decomposition become a necessity (Springel, 2005; Schaller et al., 2024; Menon et al., 2015).

In this paper, we present a new implementation of GPU acceleration in SWIFT where task management and other highly memory bound tasks are left for the CPU and compute intensive but less memory bound tasks are accelerated by the GPU. The new implementation capitalises on over-lapping CPU-GPU communications with GPU computations and tasks are bundled into large groups of tasks such that the CPU-GPU communications are optimised for high bandwidth and kernel launch overheads are minimised. This paper is structured as follows:

In Section 2 the methodology used in the GPU accelerated SWIFT solver is presented where the SPH method is outlined in Section 2.1, task-parallelism in SWIFT is discussed in Section 2.2 and the method for GPU acceleration is presented in Section 2.3. In Section 3 the speedups achieved for task computations are presented where 3 different systems built with different hardware architectures are used for the analysis. In Section 4 the GPU accelerated solver’s performance for full simulations is assessed and compared to the original SWIFT CPU solver. Current limitations of the GPU accelerated solver are also discussed in Section 4 before conclusions and future work are discussed in Section 5.

## 2 METHODOLOGY

### 2.1 The governing equations

#### 2.1.1 The SPH interpolation:

Within the SPH scheme, the computational domain is discretised into Lagrangian particles which move through space according to the governing equations. A quantity  $Q$  of a particle  $i$  may be interpolated as

$$\widehat{Q}_i = \sum_j \frac{m_j}{\rho_j} \mathbf{Q}_j W_{ij}. \quad \text{Eq. 1}$$

where  $W$  is the smoothing kernel with  $W_{ij}=W(r_{ij}, h)$ ,  $r_{ij}=|\mathbf{r}_j-\mathbf{r}_i|$  with  $\mathbf{r}$  being the position vector,  $m$  is mass of the particle,  $\rho$  is the mass density,  $h$  is the smoothing length and  $j$  represents the neighbouring particles. In SWIFT,  $h$  is variable and is a particle quantity. For SPH with uniform  $h$ , neighbouring particles are included in the summation if the distance between them and particle  $i$  is smaller than  $\varepsilon h$  where  $\varepsilon$  is a constant which can be adjusted to adjust the width of the kernel used for the interpolation.  $\varepsilon$  is usually set to between 1 and 2 and examples of widely used kernels are the cubic spline and Wendland kernels. In typical SWIFT applications which require variable  $h$ , particle densities vary greatly, and a particle’s density is directly linked to its smoothing length. As such  $h$  is evaluated individually for each particle following the process described in Section 2.1.2.

From Eq. 1 the fluid density may be interpolated as,

$$\widehat{\rho}_i = \sum_j m_j W_{ij}. \quad \text{Eq. 2}$$

Similarly to interpolations of a function, its spatial derivatives may be approximated as

$$\nabla \cdot \widehat{\mathbf{Q}}_i = \frac{1}{\rho_i} \sum_j m_j \mathbf{Q}_j \cdot \nabla W_{ij}. \quad \text{Eq. 3}$$

$$\nabla \times \widehat{\mathbf{Q}}_i = \frac{1}{\rho_i} \sum_j m_j \mathbf{Q}_j \times \nabla W_{ij}. \quad \text{Eq. 4}$$

SWIFT offers a range of approaches for modelling hydrodynamics using these SPH interpolations such as the minimal formulation based on (Price, 2012) and the GADGET 2 formulation based on (Springel, 2005). However, the default recommendation is to use the SPHENIX (Borrow et al., 2022) formulation which is more suited to SWIFT’s major use-cases (galaxy formation applications). As such, for GPU acceleration the focus is on the most compute-bound aspects of the SPHENIX scheme, namely the “density”, “force” and “gradient” loops which solve the continuity and momentum equations. Full details of the solver implementation in SWIFT can be found in (Schaller et al., 2024). The GPU accelerated parts of the solver are summarised in the following subsections.

#### 2.1.2 The density loop:

In SWIFT, the variable smoothing length and density of a particle are coupled via spatial interpolations which solve for them iteratively such that an estimate of the smoothing length is arrived at which ensures all particles interact with a pre-defined weighted number of neighbouring particles (Price, 2012). This ensures the SPH interactions are accurate but also computationally efficient. First, the particle number density  $n$  and its gradient with respect to the smoothing length are evaluated for all particles in the domain via

$$\widehat{n}_i = \sum_j W_{ij}, \quad \text{Eq. 5}$$

$$\frac{d\widehat{n}_i}{dh} = - \sum_j \left( \frac{n_d}{h_i} W_{ij} + \frac{r_{ij}}{h_i} \nabla_i W_{ij} \right). \quad \text{Eq. 6}$$

where  $n_d$  is the number of spatial dimensions for the interpolation.

The mass density is then calculated using Eq. 2 and a Newton-Raphson scheme is used to iteratively solve for Eq. 5 and Eq. 6 until the difference between the expected particle number density and the predicted value is within a small threshold, relative to expected density, of  $10^{-4}$ . The “density” tasks in SWIFT *only* involve the initial interpolations in Eq. 5 and Eq. 6 whilst the iterative solution to find the optimal smoothing length is performed in another “ghost” task routine. The ghost routine is left for the CPU to compute as it is only compute intensive for the first time step when the predicted and expected densities are disparate where a few (less than 10) iterations are required for convergence. For the remainder of the simulation, the time required to compute these ghost tasks becomes insignificant in comparison to the main SPH loops.

### 2.1.3 The gradient loop:

In this loop, the dissipative terms in the momentum equation are evaluated using an artificial viscosity formulation based on (Cullen & Dehnen, 2010) adopted in the SPHENIX scheme (Morris & Monaghan, 1997) where the artificial viscosity is a particle-carried quantity evolved through time in a manner which decays when a particle is not near shock regions. The viscous term reads

$$\frac{d\mathbf{v}_i}{dt}_{visc} = - \sum_j m_j \frac{v_{ij}}{2} (f_i \nabla_i W_{ij} + f_j \nabla_i W_{ij}), \quad \text{Eq. 7}$$

and  $f$  is the  $h$ -factor which accounts for non-uniform  $h$  written as

$$f_i = 1 + \frac{h_i}{n_a \hat{\rho}_i} \frac{d\hat{\rho}_i}{dh}, \quad \text{Eq. 8}$$

$$v_{ij} = \frac{\alpha_{v,ij} \mu_{ij} v_{sig,ij}}{\hat{\rho}_i \hat{\rho}_j}, \quad \text{Eq. 9}$$

$$v_{sig,ij} = c_{s,i} + c_{s,j} - \beta \mu_{ij}, \quad \text{Eq. 10}$$

$$\mu_{ij} = \begin{cases} \frac{v_{ij} \cdot \mathbf{r}_{ij}}{|\mathbf{r}_{ij}|} & \text{if } \mathbf{v}_{ij} \cdot \mathbf{r}_{ij} < 0 \\ 0 & \text{otherwise} \end{cases}, \quad \text{Eq. 11}$$

where the artificial viscosity parameter  $\alpha$  is evolved in time via

$$\begin{aligned} \alpha_{v,i}(t + \Delta t) \\ = \alpha_{v,i}(t) - \alpha_{v,loc,i} \exp\left(-\frac{lc_{s,i}}{H_i} \Delta t\right). \end{aligned} \quad \text{Eq. 12}$$

where the kernel cut-off radius  $H_i = \gamma_k h_i$  and the non-dimensional viscosity decay length  $l=0.05$  and

$$\alpha_{v,loc,i} = \alpha_{v,max} \left( \frac{S_i}{v_{sig,ij}^2 + S_i} \Delta t \right), \quad \text{Eq. 13}$$

$$S_i = H_i^2 \max(0, -\dot{\nabla} \cdot \mathbf{v}_i), \quad \text{Eq. 14}$$

$$\dot{\nabla} \cdot \mathbf{v}_i(t + \Delta t) = \frac{\nabla \cdot \mathbf{v}_i(t + \Delta t) - \nabla \cdot \mathbf{v}_i(t)}{\Delta t}. \quad \text{Eq. 15}$$

The final value of the artificial viscosity term is then evaluated as

$$\alpha_{v,ij} = \frac{\alpha_{v,i} + \alpha_{v,j}}{2} \cdot \frac{B_i + B_j}{2}. \quad \text{Eq. 16}$$

### 2.1.4 The force loop:

In the force loop, the acceleration due to pressure gradients and the rate of change of energy are evaluated using

$$\frac{d\mathbf{v}_i}{dt} = - \sum_j m_j \left( \frac{f_i P_i}{\rho_i^2} \nabla_i W_{ij} + \frac{f_j P_j}{\rho_j^2} \nabla_i W_{ij} \right), \quad \text{Eq. 17}$$

$$\frac{du_i}{dt} = \sum_j m_j \frac{f_i P_i}{\rho_i^2} v_{ij} \cdot \nabla_i W_{ij}, \quad \text{Eq. 18}$$

where  $u$  is internal energy.

Artificial thermal conduction is also used in the SPHENIX formulation (Borrow et al., 2022), which is added into Eq. 18 as

$$\begin{aligned} \frac{du_i}{dt}_{diff} = \sum_j \alpha_{c,ij} v_{c,ij} m_j (u_i \\ - u_j) \frac{f_{ij} \nabla_i W_{ij} + f_{ij} \nabla_j W_{ji}}{\rho_i + \rho_j}, \end{aligned} \quad \text{Eq. 19}$$

with

$$\alpha_{c,ij} = \frac{P_i \alpha_{c,i} + P_j \alpha_{c,j}}{P_i + P_j} \quad \text{Eq. 20}$$

$$\begin{aligned} \frac{d\alpha_{c,i}}{dt} = \beta_c H_i \frac{\nabla^2 u_i \alpha_{c,i}}{\sqrt{u_i}} \\ - (\alpha_{c,i} - \alpha_{c,min}) \frac{v_{c,i}}{H_i}, \end{aligned} \quad \text{Eq. 21}$$

$$v_{c,ij} = \frac{|\mathbf{v}_i \cdot \mathbf{r}_{ij}|}{|\mathbf{r}_{ij}|} + \sqrt{2 \frac{|P_i - P_j|}{\rho_i + \rho_j}}, \quad \text{Eq. 22}$$

where

$$\alpha_{c,i} = \begin{cases} \alpha_{c,i} & \alpha_{c,i} < \alpha_{c,max} \\ \alpha_{c,max} & \alpha_{c,i} > \alpha_{c,max} \end{cases}, \quad \text{Eq. 23}$$

$$\alpha_{c,max,i} = \alpha_{c,max,i} \left( 1 - \frac{\alpha_{v,max,i}}{\alpha_{v,max}} \right). \quad \text{Eq. 24}$$

## 2.2 Task-parallelism with SWIFT

In SWIFT simulations, the computational domain is split into cubic cells each of which contains a set of SPH particles. The computations themselves are split into tasks where each task only performs particle interaction computations for particles in one cell or for particles in a pair of neighbouring cells. This allows for computational parallelisation to be implemented such that each computational thread can act on an *individual* task which is the essence of task-parallelism. In the following, the major difference between task-parallelism and data-parallelism is discussed. The full methodology for task-based parallelism in SPH has been presented in (Schaller et al., 2024) and (Gonnet, Chalk & Schaller, 2016).

### 2.2.1 Task parallelism:

With conventional data-parallelism, computations are performed in a process-by-process manner. Here, each process required for the simulation, e.g. computation of particle accelerations, time integration and MPI communications, must be completed before computations from another process may be executed as illustrated in Figure 1.

Therefore, with data-parallelism, *all* the available compute threads must perform computations from the same process (acting on different elements of the same data set). It is easy to see how this can detriment performance in cases where the computational load is imbalanced. For example, due to the Lagrangian nature of SPH, particles move through space and one thread can be acting on a cell containing two or three particles whilst another thread can be acting on a cell containing hundreds of particles as illustrated in Process<sub>1</sub> of Figure 1 where the size of data operated on is different for each thread. With data-parallelism, the thread acting on the relatively empty cell will have to wait idly whilst in task-parallelism the thread can simply grab another task which allows all threads to remain busy until all tasks are executed as shown in Figure 2. Process<sub>2</sub> in Figure 1 illustrates an example where there is not enough data to split evenly between available threads and where the overheads of creating a parallel region could be greater than the benefit of parallelisation.

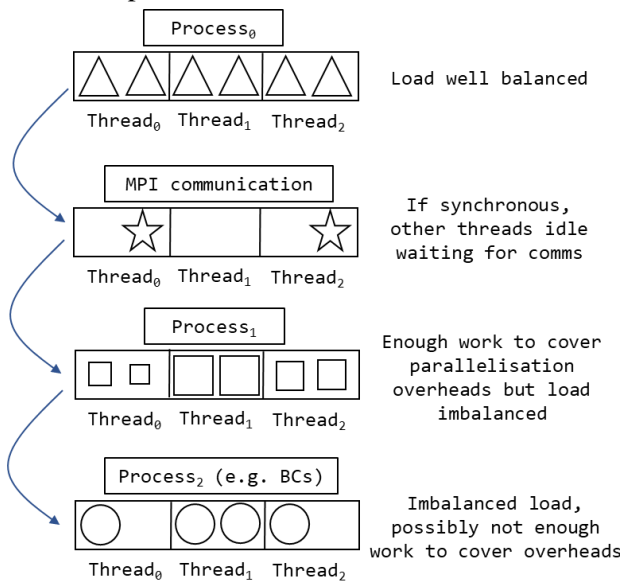


Figure 1. Illustration of data parallelisation where all threads operate on pieces of data performing the same operation concurrently and the computation is performed one process at a time

In a naïve task-parallel implementation, task queues could be filled unequally as shown in Figure 2 however in SWIFT, a thread with a relatively empty queue “steals” tasks from other over-filled queues which ensures near-perfect load balancing (Schaller et al., 2024).

As shown in Figure 2, with task-parallelism, one compute thread may be computing accelerations for particles in one cell (triangle shaped task) whilst another thread may be integrating particles in another cell through time (circle shaped task) in

tandem with another thread interleaving MPI communications with these computations.

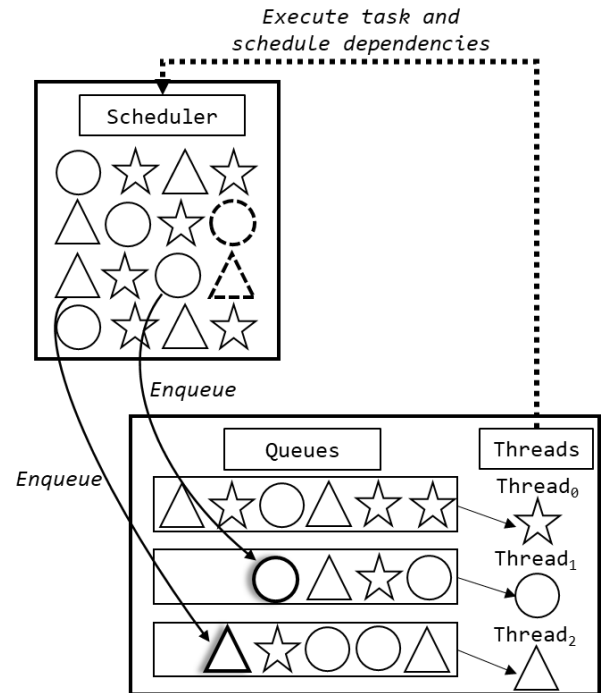


Figure 2. Illustration of task parallelism where a scheduler pools tasks from different processes and enqueues them in pipelines for all the available threads. Threads execute tasks from different processes concurrently, then unlock their dependent tasks before moving onto the next task in their queue.

For computational processes which are only required in small areas of the domain, e.g. wall boundary conditions (BCs), task-parallelism can significantly improve scalability and reduce thread idle time due to these relatively small computations being pooled with tasks from other processes to ensure compute threads always have a large pool of tasks available. This is used effectively in the UinTAH solver which leverages task-parallelism to efficiently solve multi-physics problems (Meng & Berzins, 2014) (requiring multiple solvers with different discretisations and compute loads). Communications are also easily made asynchronous with task-parallelism where they may be initiated by one thread asynchronously which can then move onto another compute task whilst the communication is finalised by the network controller.

In SWIFT, race conditions are avoided through the implementation of dependencies in-between different task types which ensure dependent tasks are only scheduled for execution after their dependency tasks are executed as shown in Figure 2. Locks are also enforced on a task’s data to ensure that only the thread executing the task can access its data. Details of these mechanisms may be found in (Gonnet,

Chalk & Schaller, 2016) where SWIFT’s task engine, QuickSched, is also discussed in detail.

### 2.2.2 The SWIFT SPH tasks:

In SWIFT, tasks are categorised into types and sub-types. The major task types are self and pair tasks. Self tasks perform computations on particles contained within a cell using data only from within that cell whilst pair tasks perform computations on a pair of cells using data from one cell to update data

on the other cell and vice-versa as illustrated in Figure 3. SWIFT has a wide range of task sub-types as discussed in (Schaller et al., 2024) but the major *SPH* task sub-types are the “density”, “gradient” and “force” task sub-types which compute the loops discussed in Section 2.1. In general, they are SPH summations which perform computationally intensive but memory-bound interactions between all particles contained in one cell or with all particles in neighbouring cells.

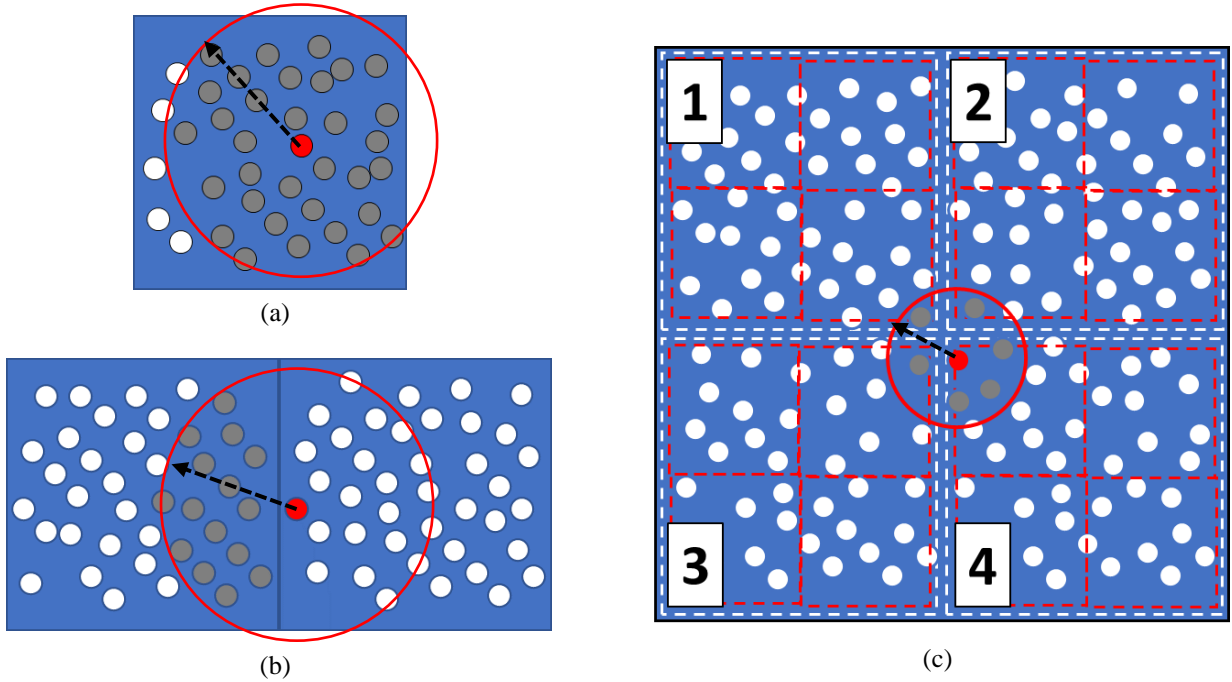


Figure 3. SWIFT SPH task types: (a) Self tasks where all particles in one cell interact with neighbouring particles (within  $\epsilon h$ ) in the same cell. (b) Pair tasks where all particles in one cell interact with neighbouring particles in adjacent cells. (c) Sub-self task. In SWIFT, tasks are usually created to act on a cell at a high level of the cell tree. As the high-level “parent” cell contains too many particles for efficient neighbour finding, the task recurses through the cell’s daughter cells (4 cells in 2D outlined in dashed white lines). If the cell’s daughter cells are still too large for efficient particle interactions SWIFT recurses again until the maximum smoothing length of particles in a cell is just smaller than the cell width divided by  $\epsilon$ . At this point SWIFT computes the resulting self and pair interactions using the optimum number of neighbours. In the example above, two recursions were executed. The first recursion split the cell into cells 1 to 4 (outlined in dashed white lines) and the second split each of these cells into 4 more quadrant cells (outlined in dashed red lines). The red particle in daughter cell 4 for example, will have self interactions with other particles *only* in its quadrant cell of cell 4 and will also have pair interactions *only* with particles in other quadrant cells of cell 4 and particles in neighbouring quadrant cells of cells 1, 2 and 3 within a distance of  $2h$ . In 3D, a cell will have eight daughter cells (each daughter cell will have one self interaction and seven pair interactions).

Other tasks include the “kick” and “drift” tasks for time integration, “sort” tasks which sort particles along the axis connecting two neighbouring cells in a pair task to identify which particles in the two cells are likely to interact prior to performing the computations (Schaller et al., 2024) which significantly optimises the pair task interactions and other “ghost” tasks which finalise the density, gradient and force tasks by performing minor particle-wise computations not involving neighbours, see (Schaller et al., 2024) for details. The aforementioned task subtypes are of low computational intensity  $O(N)$  where  $N$  is the number

of particles on which the tasks act and as such are not ideally suited for GPU acceleration via our GPU offloading approach and are left for the CPU to execute; the data for these low intensity tasks is on CPU memory, as is the data for all tasks, therefore the path of access to their data for CPU threads is much shorter than the path for the GPU threads. As such, they can be executed rapidly on CPU threads whilst GPU threads are busy executing the compute intensive density, gradient and force tasks which are  $O(N^2)$ .

The overheads of task creation and management could be significant if tasks are too fine-grained.

Thus, “tasking” overheads must be minimised to allow the solver to achieve the desired gains in time to solution. As such, SWIFT’s tasks are designed to perform the particle-wise computations for all particles in a large parent cell, Figure 3 (c), which contains several daughter cells of the optimal size for SPH computations ( $2h$ ). Tasks acting on these parent cells are called sub-tasks and in sub-tasks a CPU thread recursively loops through their daughter cells via a pre-defined recursion process where for each daughter cell the necessary self and pair interactions (with itself and other neighbouring “sister” cells) are performed. Typically, sub-tasks act on parent cells several levels above the optimal cell size. This is due to most SWIFT applications having large variations between neighbouring particle smoothing lengths. The cell tree is created at the beginning of the simulation and re-created when the particle distribution has changed significantly according to criteria discussed in (Gonnet et al., 2013). During cell tree creation the code recurses through a few top-level cells splitting them into daughter cells and organising particles into the daughters at each level created. The recursion continues until the daughter cells contain no particles at which point the recursion stops. The top-level cells are defined once at the beginning of the simulation and act as the seed from which the parent cells used in sub-tasks are created from which the daughter cells are then created. Additionally, for all pair interactions a pre-sorting step (Willis et al., 2018) is conducted prior to computing the particle interactions where particles in the two cells are sorted along the axis connecting the cells into lists such that particles in the neighbouring cell will only search for neighbours in these lists thereby minimising wasted effort which would result from searching for neighbours through all the particles in the neighbouring cell. The pre-sorting step is a pseudo-Verlet list algorithm as detailed in (Gonnet et al., 2013). Further details of the cell splitting and sub task mechanisms are also discussed in (Gonnet et al., 2013).

## 2.3 GPU acceleration

GPU acceleration is extremely beneficial for highly parallelisable and compute-bound problems and in the following sub-sections, different approaches are discussed for capitalising on the capabilities of GPUs for SPH simulations.

### 2.3.1 GPU acceleration for SWIFT

SWIFT’s SPH tasks are designed to be fine-grained to maximise efficiency by minimising thread idle time. Since threads do not have to wait for all tasks belonging to a certain type to be completed before

moving on to other task types. All available compute threads can fetch tasks from their queues until all tasks are completed. The optimal size of these tasks is problem dependent but typically the optimal task size is  $O(10^3)$  particles. This task size is efficient for parallelisation on CPUs as tasks fit well on CPU cache (especially if the recursive mechanism is employed to identify daughter tasks acting on  $O(10^2)$  particles) and memory access of small data packets is generally much faster on CPUs than it is on GPUs. However, in order to ensure efficient GPU off-loading of SWIFT’s tasks, an approach is required which can maximise the efficiency of:

- 1- CPU-GPU communications. It is much more efficient to transfer one large packet of data stored in simple 1D arrays than it is to transfer multiple small packets of data stored in complex structures as this allows the interconnect to achieve much higher transfer speeds and minimises latency (Corporation, 2025).
- 2- Data transfer from global GPU memory to the GPU registers. This is much more efficient when large packets of contiguous data are transferred as this minimises memory transactions and helps saturate device memory (DRAM) bandwidth improving transfer speeds (Corporation, 2025).
- 3- Computations on the GPU. It is also more efficient to instruct the GPU to launch one kernel acting on a large block of data than it is to launch several kernels acting on smaller packets of data. This minimises kernel launch overheads and also benefits DRAM bandwidth saturation which is a major concern with GPU programming (Corporation, 2025).

### 2.3.2 Heterogeneous SWIFT with task-parallelism

As discussed in Section 2.2.2, not all of SWIFT’s tasks would benefit from GPU acceleration and with the concerns raised in Section 2.3.1 in mind, a bespoke approach is proposed to off-load SWIFT’s tasks to the GPU as follows.

#### 2.3.2.1 Host-side data packing:

On the SWIFT host code, threads performing SPH tasks access the particle data on which they will act by first de-referencing a pointer to find the location in memory of a “cell” struct corresponding to the cell which contains the particles. The cell struct contains an array of “part” structs each of which contains small  $3 \times 1$  arrays storing a particle properties. Transferring data of this form directly to the GPU is intractable and requires nested CPU to GPU copies, first for the particle structs and then for the cell struct which contains the particle structs.

Therefore, we create a new SWIFT task sub-type, which we call “pack\_d”, “pack\_f” and “pack\_g” tasks and these replace the density, force and gradient tasks. Pack tasks do not perform computations and instead, copy the data for the relevant SPH loop task from its original “struct of arrays of structs of arrays” to the form of an array of structs. For each task sub-type (density, force or gradient) an array is constructed such that each index of the array corresponds to an individual particle populated with the particle data required for the computation of several tasks. The index of the first and last particles for each SPH task is saved in memory such that the indices can be used later to control which particles interact with which particles in the array. Indices in this array each correspond to a struct of the form:

```
/*struct containing particle data required
for density loop*/
Typedef struct part_send_d{
    float4 x_p_h; //particle position vector
and smoothing length
    float4 u_m; //particle velocity vector
and mass
    int2 cf_cl; //cf index of first particle
in the cell, cl index of last particle in
cell
} part_send_d;
```

where `float4` and `int2` are datatypes in cuda/HIP which store four 32-bit floats and two ints contiguously and allow for vectorisation of load/store instructions to and from the GPU’s DRAM to core-local registers. Vectorisation helps saturate the memory bandwidth with efficient transactions maximising bandwidth and computation efficiency. Similar `part_send_f` and `part_send_g` structs are defined to contain data for the force and gradient loops, respectively.

Sending the data one task at a time ( $O(100)$  bits)) on pathways designed for  $O(100)$  GB/s) throughput is extremely inefficient as this cannot saturate the CPU-GPU communication, introducing the significant over-head and latency of hundreds of thousands of memcpys to the GPU per time step; memcpys are instructions for data transfer to and from the GPU. An approach is therefore implemented where task data is bundled into larger data sets and transferred to the GPU asynchronously as discussed in the following sub-section.

### 2.3.2.2 Controlling GPU data transfers and computations via instruction streams

The `part_send` arrays are designed to contain data for a pack of tasks containing  $S_p$  tasks where the pack size  $S_p$  is designed to be pre-defined in a manner

which optimises data transfers and computations for the available hardware depending on the CPU-GPU interconnect, the GPU memory access speeds and the number and speed of GPU compute cores. SWIFT is parallelised using pthreads which means CPU threads are mostly unaware of what other threads are doing and operate independently unless pthread synchronisation or communication directives are called. As such each CPU host thread instructs the GPU independently and requires its own `part_send` arrays in which to pack the task data. To prevent excessive calls to the computationally expensive process of allocating GPU memory, the GPU memory allocated to each host thread is allocated once at the start of the simulation. The size of the memory allocated to each thread is proportional to the number of particles offloaded to the GPU per offload cycle,

$$N_{offload} = \frac{S_p N_p}{N_c}, \quad \text{Eq. 25}$$

where  $N_p$  is the total number of particles in the simulation and  $N_c$  is the number of cells the domain would be divided into if the domain was divided into cells with a uniform volume of  $8h^3$  assuming a uniform constant  $h$  for all particles. The memory allocated per host thread to store the particle data on the GPU is

$$M_t = 4n_{loops}N_{offload}M_{struct}, \quad \text{Eq. 26}$$

where  $M_{struct} \sim 44$  bytes is the average size of the `part_send` and `part_recv` structs for the density, gradient and force computations and `part_recv` is a struct similar to `part_send` used to send the computation results back to the CPU and  $n_{loops} = 3$  is the number of loops off-loaded to the GPU (density, gradient and force). The coefficient of 4 accounts for the 2 task types (self and pair) and the 2 data types (`part_send` and `part_recv`).

### 2.3.2.3 Adapting task bundling and instruction streams to SWIFT’s task scheduler

To maximise concurrency of GPU computations with CPU-GPU communications, many GPU-accelerated codes leverage streaming of instructions which is a method by which each host thread issues groups of instructions to the GPU in different instruction streams where instructions issued in one stream may be executed concurrently with instructions in another stream. Figure 4 illustrates how this concept may be used to virtually hide the cost in time-to-solution of CPU-GPU data transfers underneath GPU computations.

In each stream, a host to device memory copy, referred to as memcpy, ( $HD_n$  where  $n$  is the stream ID) is first issued to instruct the GPU to copy the required task data *asynchronously* with other instructions in different streams. This is followed by instructions to execute the required task computations ( $Kernel_n$ ) on that data and then by instructions to retrieve the tasks' results data to the CPU via another asynchronous device to host memcpy ( $DH_n$ ). After the instructions are issued, the GPU is left to perform the memory transactions and compute kernels as and when enough resources are available (GPU copy engines, CPU-GPU link bandwidth and GPU memory and compute cores). If the ratio of computations to memory transactions is sufficiently large, the GPU will be able to hide HD/DH memcpys underneath kernel computations which can greatly improve off-load efficiency as shown in Figure 4 where a dashed red box highlights

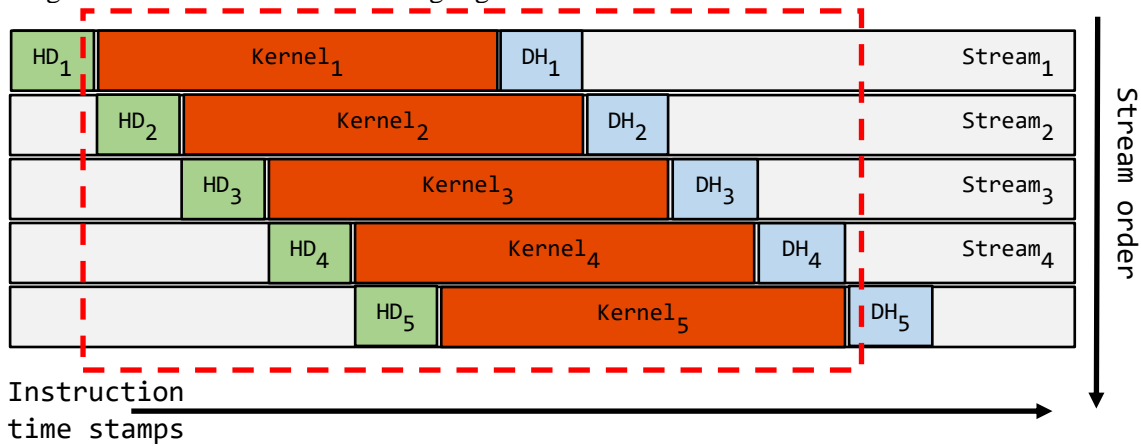


Figure 4. Timeline of execution for GPU operations. The schematic illustrates different data transfers and computations executed concurrently by the GPU as issued by one CPU host thread in different instruction streams. HD denotes host-to-device transfer, while DH denotes device-to-host transfer. The host is the CPU node, while the device is the GPU.

Having identified a method for controlling GPU-offloading such that communications could be hidden underneath FLOPS, this must now be incorporated within SWIFT's task-parallel solver in a manner which is minimally disruptive to the solver's overall scalability. SWIFT's scheduler controls the creation and assignment of tasks into queues where each CPU/host thread has its own queue as illustrated in Figure 5.

In our off-loading approach, we first add the pack tasks discussed in Section 2.3.2.1 to the scheduler such that they are scheduled for execution with other tasks (as and when their dependencies are met, tasks are quasi-randomly placed (Gonnet, Chalk & Schaller, 2016) into several queues, each of which is assigned to a CPU thread). Then, if a CPU thread receives a regular (non-GPU-accelerated) SWIFT task:

a time in the offload process where all CPU-GPU communications are performed concurrently with GPU computation kernels.

To control how and when data is transferred to the GPU we define a new parameter, the bundle size  $S_b$ , which is the number of tasks we offload to the GPU via each instructions stream. I.e., when we offload  $S_p$  tasks, we first split them into  $S_b$  tasks where  $S_b < S_p$  meaning that for each GPU offload we launch  $S_p/S_b$  kernels and issue HD and DH memcpys for each kernel separately. Therefore, the  $S_p$  tasks off-loaded by each host thread are split into bundles each containing  $S_b$  tasks in a manner which enables the optimisation of the off-load process such that streams are used effectively to hide CPU-GPU communications. Our implementation of task bundling is discussed in the following Section.

- 1- The thread executes the task.
- 2- Its data and dependencies are unlocked.
- 3- The thread moves on to execute the next task in its queue.

If on the other hand a thread receives a pack task, the procedure is slightly more involved and is described as follows:

#### Packing and off-load:

- 1- The thread packs the task's data into a large array of `part_send` structs designed to contain the particle data for  $S_p$  tasks,  $S_p=6$  in Figure 5 for illustration purposes.
- 2- If the number of tasks a thread has packed is smaller than  $S_p$  tasks, the thread moves on to the next task in its queue.
- 3- If the thread has packed  $S_p$  tasks, it triggers the GPU offload process and splits the packed tasks

into smaller bundles each containing  $S_b$  tasks which are offloaded to the GPU via different instruction streams as and when the GPU's copy engines are available, in Figure 5  $S_b=2$  for illustrative purposes.

- 4- The GPU is then instructed by the thread to *asynchronously* copy the data for each task bundle in a separate stream.
- 5- The GPU then launches compute kernels to perform the computations on each task bundle

from within the same instruction stream such that an instruction stream contains the memcopy instructions of some data and the computation instructions to act on that *same* data (the kernel).

- 6- Asynchronous memcopy instructions are then issued to copy the results of the computations back to the CPU in the *same streams* from which the computation kernels were launched.

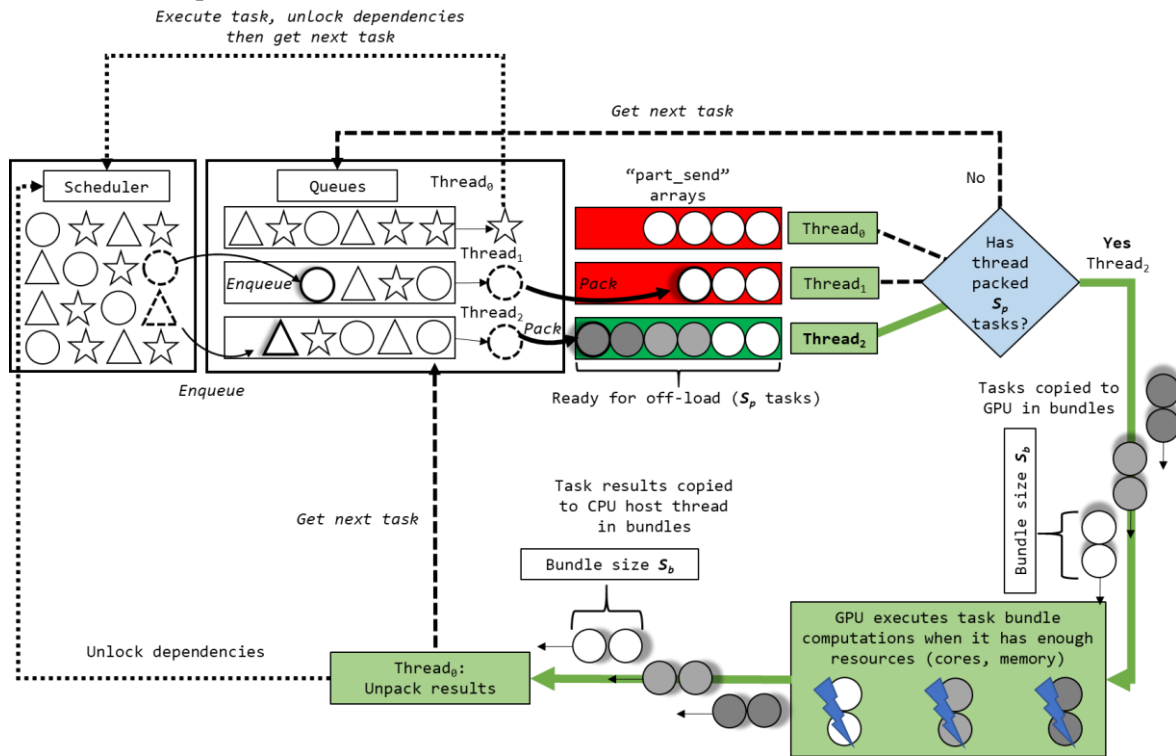


Figure 5. GPU-offload mechanism for SWIFT tasks. Circles in this image represent pack tasks where the data required for the computations is packed into arrays of `part_send` structs. Once a thread has packed the data for  $S_p$  tasks the offload process begins.

## Unpacking

Once the CPU thread has the results, it begins unpacking the results from each stream when it receives a bundle such that the GPU is working on the next bundle whilst the CPU thread is unpacking the results of the previous bundle. This additional level of asynchrony is enacted by looping through the task bundles and issuing one `cudaEventSynchronize()` call for each bundle. The `cudaEventSynchronize()` function instructs the CPU to wait at the function call until the GPU has flagged that a "CUDA event" has occurred. In our implementation, a CUDA event is setup such that it occurs after each asynchronous DH memcopy instruction in step 6. Since the events are issued after the DH memcopy the host CPU thread will wait until the data has been copied onto CPU memory. This ensures that the results data for a task bundle has been copied to CPU memory before it is unpacked

whilst allowing the CPU to unpack results as and when they are ready. i.e., the CPU thread does not have to wait until all the GPU memcpys are complete which would be the case when using the more stringent `cudaDeviceSynchronize()` function which forces the host CPU thread to wait until *all* previously issued GPU instructions have been completed. Rather, it waits for each individual bundle and is able to unpack the results whilst the GPU is busy performing computations or whilst the results data for another bundle is being transferred back to the CPU. This provided ~10% speedup in unpacking time in comparison to using the more stringent `cudaDeviceSynchronize()` barrier which forces the CPU thread to wait until *all* GPU operations issued by that thread are complete. After all bundles are unpacked, the data and task dependencies are then unlocked and the thread moves onto the next task in its queue.

In the DH memcopy and unpacking process, a different data type is used to minimise the size per task of DH communications by only retrieving the results which the GPU has written to (the computation results) and *not* the data the GPU read from. Similarly to the `part_send` structs, we define a `part_rcv` struct of the form:

```
typedef struct part_rcv_d{
  /*Density information: Density,
  derivative of density with respect to h,
  neighbour number,
  derivative of the neighbour number with
  respect to h*/
  float4 rho_dh_wcount;
  /*Particle velocity curl vector, velocity
  divergence.*/
  float4 rot_ux_div_v;
} part_rcv_d;
```

This approach is tested for efficiency in the next section where various CPU-GPU types and configurations are used to assess its versatility.

### 3 ANALYSIS OF GPU ACCELERATED TASK COMPUTATION

The proposed GPU-accelerated solver is tested on various GPU computing systems to validate the efficiency of the new algorithms across different GP-GPU and heterogeneous computing platforms.

Table 1. Summary of systems used for the GPU acceleration tests.

System	CPUs	GPUs	CPU-GPU Link
Bede <sup>3</sup>	32 nodes with 2x IBM POWER9 32 core CPUs each and 512GB DDR4 RAM	Nvidia V100 with 32GB memory. 4GPUs per node.	NVLink 2.0 (50 GB/s)
	5 nodes with one 72 core Nvidia Grace CPU each and 480 GB LPDDR5X RAM	Nvidia H100 with 96GB memory. 1 GPU per node.	NVLink C2C (450 GB/s)
Gemini 2	1 node with two 28 core Intel Xeon Gold 6330 CPUs and 128GB DDR4 RAM	Nvidia L40 with 48GB memory. 4 GPUs per node.	PCIe4 (32GB/s)
Isambard-AI <sup>4</sup>	42 nodes with four 72 core Nvidia Grace CPUs each and 512 GB LPDDR5X RAM	Nvidia H100 with 96GB memory. 4 GPUs per node.	NVLink C2C (450 GB/s)

The analytical azimuthal velocity ( $v_\theta$ ) and pressure ( $p$ ) only vary in the  $r$  direction. The analytical solution is

$$v_f(r) = \begin{cases} 5r & 0 \leq r < 0.2 \\ 2 - 5r & 0.2 \leq r < 0.4 \\ 0 & 0.4 \leq r \end{cases} \quad \text{Eq. 27}$$

Three different systems were used for the analyses presented in this section as summarised in Table 1.

### 3.1 Numerical setup

For all results presented in this paper the test case simulated was the 3-D Gresho-Chan vortex (Gresho & Chan, 1990) SWIFT benchmark test case<sup>2</sup> using the SPHENIX scheme (Borrow et al., 2022). In this test, a cubic domain with periodic boundaries is discretised into uniformly sized particles. The domain size is  $L^3$  with non-dimensional side length  $L = 1$ .  $\varepsilon$  is set to  $\varepsilon=2$  such that the target kernel support radius is  $2\Delta x$  where  $\Delta x$  is the initial particle spacing to ensure approximately 64 particles in each cell for the self and pair interactions. For all tests presented in Section 3, the domain is split such that each cell contains roughly 64 particles. All the density, gradient and force, self and pair tasks are executed on the GPU. The particles are assigned initial velocities according to the analytical solution and the density is set to  $\rho_0=1$  with polytropic index  $\gamma=5/3$ . The axis (centre) of the vortex is parallel to the  $z$ -axis (the analytical velocity is zero in the  $z$ -direction) and the radius of the vortex  $r$  is parallel to the  $x$ - $y$  plane.

$$p(r) = \begin{cases} 5 + 12.5r^2 & 0 \leq r < 0.2 \\ 9 - 4 \ln(0.2) + 12.5r^2 - 20r + 4 \ln(r) & 0.2 \leq r < 0.4 \\ 3 + 4 \ln(2) & 0.4 \leq r \end{cases} \quad \text{Eq. 28}$$

### 3.2 Acceleration on Nvidia V100 GPU with IBM POWER9 CPU

The N8 CIR system (Bede), a relatively small-scale system on which we conduct the tests in this subsection, replicates the architecture of Summit<sup>5</sup> with

<sup>2</sup> The case is available online [www.gitlab.cosma.dur.ac.uk/swift/swiftsim](http://www.gitlab.cosma.dur.ac.uk/swift/swiftsim)

<sup>3</sup> <https://n8cir.org.uk/bede>

<sup>4</sup> <https://www.bristol.ac.uk/campaigns/bristol-supercomputing/#isambard-ai>

<sup>5</sup> <https://www.olcf.ornl.gov/summit/>

V100 GPUs connected to IBM POWER9 CPUs via a dedicated 50GB/s NVSwitch port which is over 3 times faster than the V100's 16 channel PCIe 3 port (16 GB/s). For the V100 tests, 3 different resolutions are used ( $N_p = 64^3$ ,  $128^3$  and  $256^3$  particles) to assess the scaling of GPU off-load efficiency with problem size.  $S_p$  and  $S_b$  are varied for each resolution to determine the optimum combination of off-load parameters which ensure maximum concurrency of GPU computations with CPU-GPU data transfer. Figure 6 shows the results for the velocity and pressure fields in the Gresho-Chan vortex test confirming correctness of the GPU implementation.

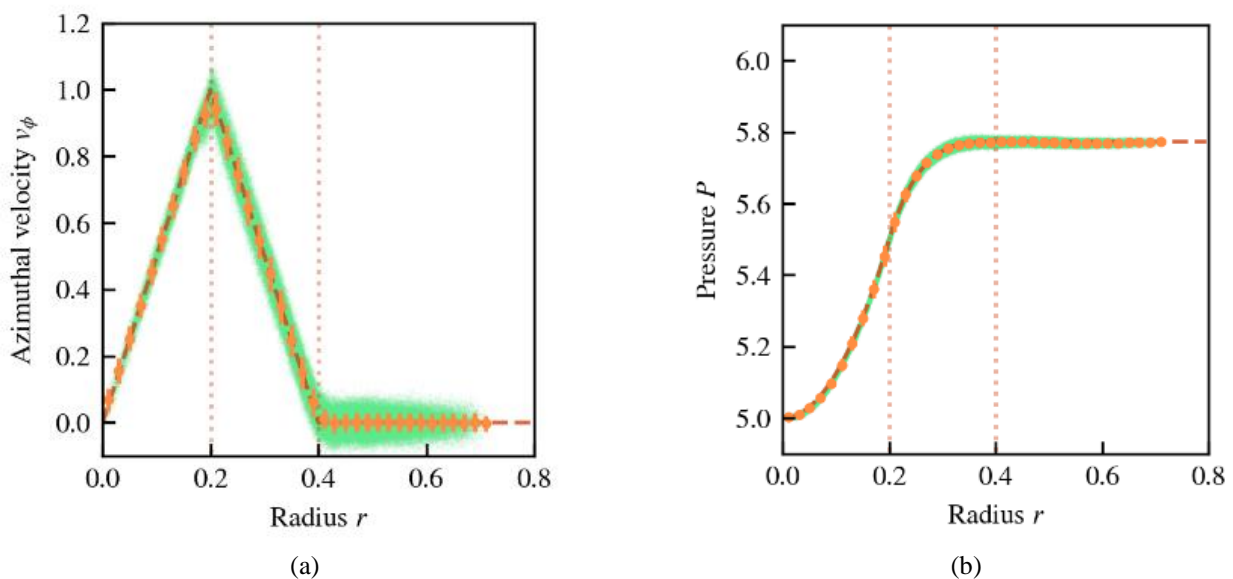


Figure 6. 3-D Gresho-Chan vortex test results using  $128^3$  particles. Velocity (a) and pressure (b) profiles are plotted against vortex radius. Dashed profiles indicate the analytical solution, green dots indicate the numerical solution predicted by SWIFT for all particles using their radial position  $r$  with respect to the vortex centre at  $t=0.1$ . The mean values are indicated by orange points with error bars indicating one standard deviation of scatter.

Figure 7 shows the compute time results for the lowest resolution test with  $64^3$  particles where increasing the total amount of data off-loaded to the GPU  $S_p$  improves the efficiency of the off-load and thereby reduces the overall data transfer and compute time. For the best performing case ( $S_p=64$ , 128 for the pair tasks and  $S_b=32$ , 64 for self tasks) the total off-load time is 0.221 s and 0.0105 s for the pair and self tasks, respectively, as compared to 0.36 s and 0.0719 s when computed on the CPU.

Increasing the resolution to  $128^3$  improves the GPU efficiency as shown in Figure 8 where the best efficiency is achieved with  $S_p=256$ , 512 and  $S_b=128$ , 256 for the pair and self tasks, respectively. The CPU times for  $N_p=128^3$  are 3.02 s and 0.534 s as compared

To assess the effects of total offload size and offload size per bundle on the efficiency of the GPU computations, a battery of tests is performed where the total number of the computations offloaded  $S_p$  and the total number of computations per bundle  $S_b$  are varied. Increasing  $S_p$  has the effect of minimising the cost of kernel launch overheads per task computed as we launch fewer kernels with increased  $S_p$ . On the other hand, having more bundles per offload (reducing  $S_b$ ) has the effect of increasing kernel launch overheads (as we launch more kernels) but allows for additional concurrency of computations and CPU-GPU communications as discussed in Section 2.3 and illustrated in Figure 4 and Figure 5.

to the most efficient GPU off-loads with 0.971 s and 0.0477 s for the pair and self tasks, respectively.

Increasing the resolution to  $N_p=256^3$  improves efficiency further as seen in Figure 9, for this test 32 CPU cores for the CPU time results and 32 host threads were used for the GPU time results. The best performing cases are for  $S_p=1024$ , 2048 and  $S_b=256$ , 512 for the pair and self tasks, respectively where the CPU times were 12.7 s and 2.14 s whilst the GPU times were 4.07 s and 0.197 s for the pair and self tasks, respectively.

To expand on the GPU performance for the sets of V100 tests, Figure 11 shows GPU activity profiles obtained using Nvidia's NSight Systems<sup>6</sup> profiler for

<sup>6</sup> <https://developer.nvidia.com/nsight-systems>

the cases with  $N_p = 64^3, 128^3$  and  $256^3$  which illustrate how the GPU executes tasks such as memcopy and computation kernels as instructed by the host. Select time windows in the computations were chosen to illustrate cases (combinations of  $N_p, S_p$  and  $S_b$ ) where concurrency of CPU-GPU communications was achieved (thereby hiding communication costs) and cases where concurrency was not achieved.

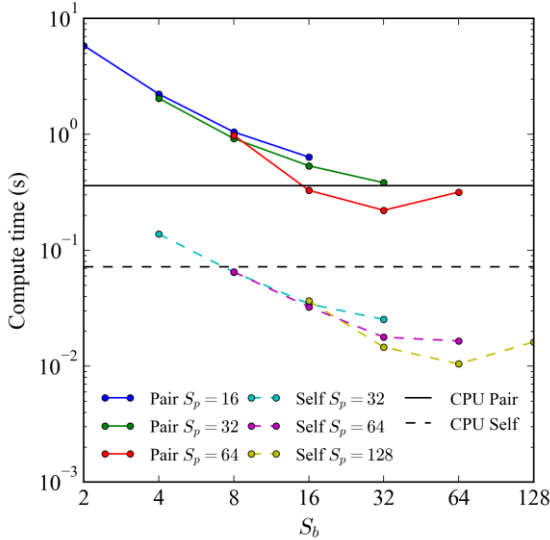


Figure 7. Variation of compute time on V100 with  $S_p$  and  $S_b$  for the case with  $N_p = 64^3$  using 16 host threads compared to CPU times with 16 threads.

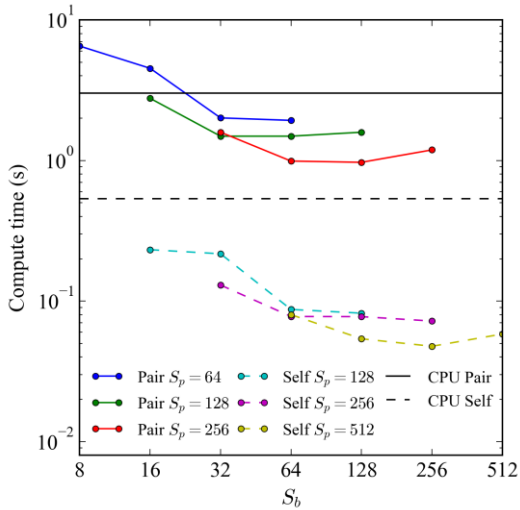


Figure 8. Variation of compute time on V100 with  $S_p$  and  $S_b$  for the case with  $N_p = 128^3$  using 16 host threads compared to CPU times with 16 threads.

Figure 11 (a) and (b) show that for the cases with  $N_p=64^3$  and  $128^3$  concurrency is achieved where memcpys are mostly hidden underneath compute kernels. However, given that only four kernels are executed per cycle demonstrates that only two bundles of tasks from two host threads are executed per offload cycle, this limits the ability of the GPU

to efficiently schedule the execution of kernels and memcpys concurrently.

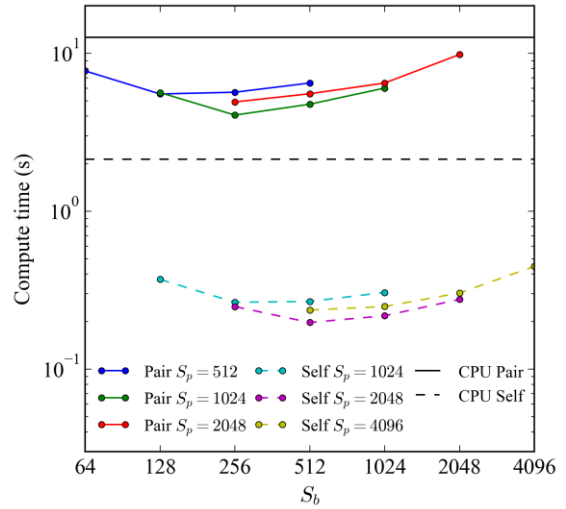


Figure 9. Variation of compute time on V100 with  $S_p$  and  $S_b$  for the case with  $N_p = 256^3$  using 32 host threads compared to CPU times with 32 threads.

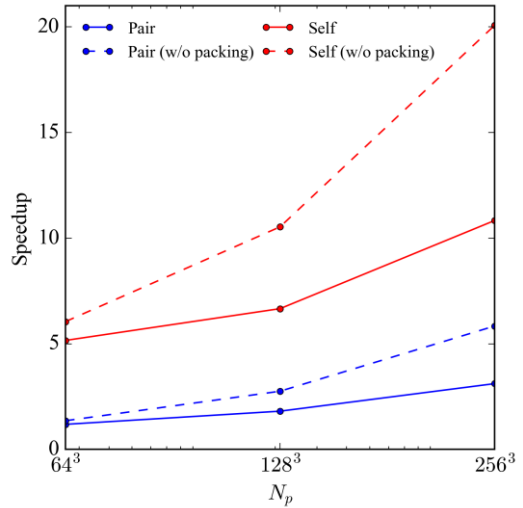


Figure 10. Speedups of self and pair tasks executed on a V100 GPU for three different values of  $N_p$ . Speedups are against 32 CPU threads.

Figure 12 on the other hand shows that for the best performing case with  $N_p = 256^3$ , data transfer and kernel execution are highly concurrent with two-way data transfers occurring concurrently and concurrent execution of kernels and memcpys. For the self task sample offload cycle in Figure 12 (a), there are eight kernels executed meaning that four bundles of tasks from two host threads are executed concurrently. For the pair tasks in Figure 12 (b), there are sixteen kernels meaning that there are tasks from four host

threads being executed in the same cycle which allows for even greater concurrency.

Table 2 highlights the GPU throughputs for computations and CPU-GPU communications for all tests presented in this sub-section and Figure 11 (c) and Figure 11 (d) show the most extreme examples presented here. For the case with  $N_p=256^3$  and  $S_p = 4096$  and  $S_b = 4096$ , memcpys and kernels are the most efficient however the overall offload time (see

Figure 9) is the longest of all tests conducted using  $N_p=256^3$  (0.448s and 9.84s for self and pair tasks respectively which is not significantly faster than the CPU time of 2.14 s and 12.7 s for self and pair tasks on 32 CPU threads). The reason why this case is slower overall than the best performing case ( $N_p=256^3$ ,  $S_p=2048$ ,  $S_b= 512$ ) is due to the fact that no concurrency between CPU-GPU communications and GPU computations was achieved.

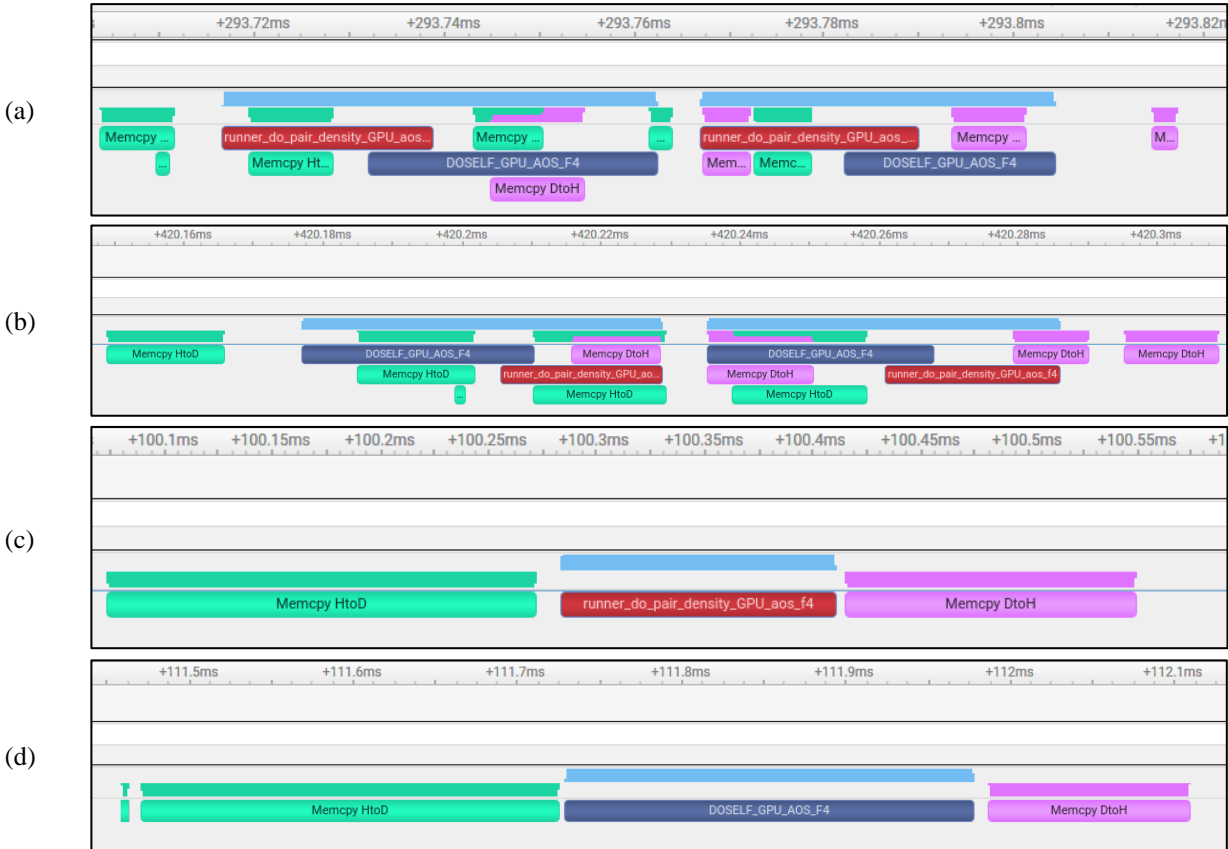


Figure 11. Profiles for a GPU offload cycle on the V100 GPU for select test cases. (a)  $N_p = 64^3$ ,  $S_p = 128$  and  $S_b = 64$  with 16 host threads. (b)  $N_p = 128^3$ ,  $S_p = 512$  and  $S_b = 256$  with 16 host threads. (c)  $N_p = 256^3$ ,  $S_p = 4096$  and  $S_b = 4096$  with 32 host threads. Green blocks represent host to device data transfer, lavender blocks represent device to host data transfer, red blocks represent kernels executing pair tasks and dark blue blocks represent kernels executing self tasks.

Further analysis presented in Table 2, illustrates that the time required to compute a task by the GPU improves as  $N_p$ ,  $S_p$  and  $S_b$  are increased and so does the memcopy throughput measured by NSight Systems which exceeds the stated 50 GiB/s throughput of the NVlink2 connection for the largest pack and bundle sizes tested. This is due to the larger computations and communications saturating the GPU’s capabilities in terms of CPU-GPU communications bandwidth and also due to the fact that kernel launch overheads are minimised; The number of GPU instructions is reduced, and the total size of the data transferred is increased, by a factor of 4. However, since no concurrency of data transfer and computations is achieved, overall off-load

efficiency is significantly deteriorated in comparison to cases where concurrency is achieved.

The best achieved speedups ( $T_{CPU}/T_{GPU}$ ) are summarised in Figure 10 which shows speedups for the 3 resolutions compared to the time for 32 CPU threads to perform the computations for consistency across resolutions. It is clear that the packing and unpacking of data on the host is taking a considerable amount of time especially for the largest test with  $N_p = 256^3$  particles where it is roughly 47% of  $T_{GPU}$ .

An issue with the packing and unpacking is that the compiler is unable to vectorise the data access due to the non-contiguous nature of the data on the host. Vectorisation of the host memory should speedup the packing and unpacking process for single precision

(32 bit) data on CPUs with 512-bit Advanced Vector Extensions (AVX-512), in theory 16 data copies can be performed concurrently on such a configuration provided the data is contiguous in memory. However, data bus limitations (latency and bandwidth) would limit the achieved speedups to significantly less than 16 times. Whilst investigating

what speedups are possible if the packing/unpacking process is vectorised is of significant interest, this requires an overhaul of the host code data structure, for the CPU solver, for other SWIFT task types which use the SPH task data and is the focus of future work.

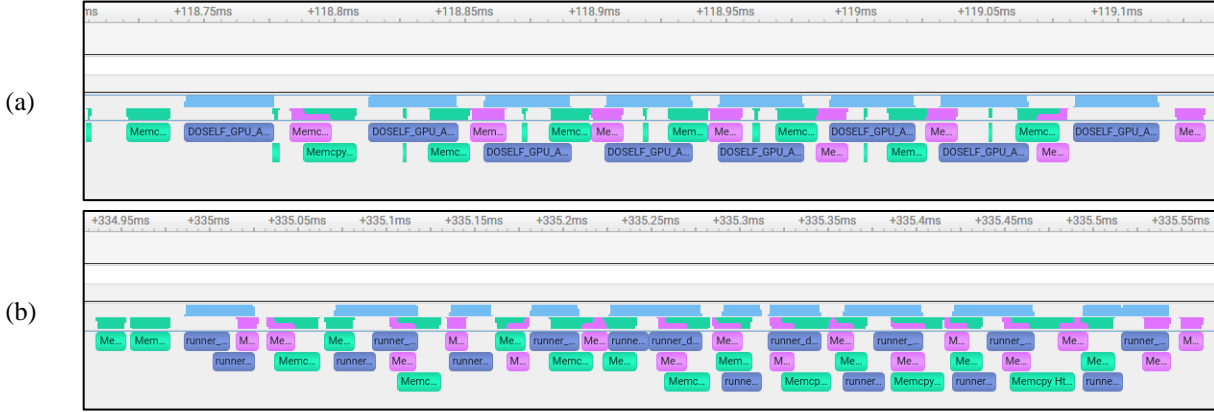


Figure 12. Profile for a GPU offload cycle on the V10 GPU for the case with  $N_p = 256^3$ ,  $S_p = 2048$  and  $S_b = 512$ . (a) Self tasks. (b) Pair tasks. Green blocks represent host to device data transfer, lavender blocks represent device to host data transfer and dark blue blocks represent kernels executing self or pair tasks.

Table 2. Average times required to complete self and pair tasks and maximum data transfer (memcpy) throughput for selected test cases with varying  $N_p$ . The columns for  $N_p=64^3$  and  $128^3$  show the best performing tests for those resolutions whilst the two columns with  $N_p=256^3$  show the best and worst performing combination of  $S_p$  and  $S_b$  for that resolution from Figure 9.

	$N_p=64^3$ ( $S_p=128, S_b=64$ )	$N_p=128^3$ ( $S_p=512, S_b=256$ )	$N_p=256^3$ ( $S_p=2048, S_b=512$ )	$N_p=256^3$ ( $S_p=S_b=4096$ )
Self kernel time/task	0.237 $\mu$ s	0.0654 $\mu$ s	0.0641 $\mu$ s	0.0664 $\mu$ s
Pair kernel time/task	0.285 $\mu$ s	0.0816 $\mu$ s	0.0859 $\mu$ s	0.0293 $\mu$ s
Memcpy throughput	20 GB/s	45 GB/s	47 GB/s	56 GB/s

### 3.3 Acceleration on architectures with conventional PCIe connections

In this section, the GPU accelerated SWIFT solver is tested on the University of Manchester compute system (Gemini 2) with Nvidia’s L40 GPUs, where connectivity to CPUs is via 16 PCIe 4 channels which can deliver 32 GB/s CPU-GPU data transfer speeds. The setup for these tests is identical to the setup for the tests in Section 3.4.

For the L40 GPU runs the performance was significantly affected by the speed of the CPU-GPU connection. Figure 13 shows that whilst the self tasks were still faster on the L40 GPU, in comparison to 32 Intel Xeon Gold 6330 CPU threads, the pair tasks

were in general slower on the GPU in comparison; the best achieved time for pair task completion ( $S_p=2048$  and  $S_b=2048$ ) was 21.2 s in comparison to 10.8 s. For the self tasks the best achieved time was 0.458 s in comparison to 1.62 s on 32 CPU threads. This is due to the fact that the GPU is unable to hide the CPU-GPU data transfers under computations due to the much slower PCIe connection being unable to keep up with the computational throughput of the L40 GPU. Since the pair tasks require twice the amount of data as for the self tasks and the number of particle interactions is generally much smaller, especially for pair tasks acting on two cells connected by a corner, for example, the CPU-GPU data transfer speed becomes the dominant bottleneck.

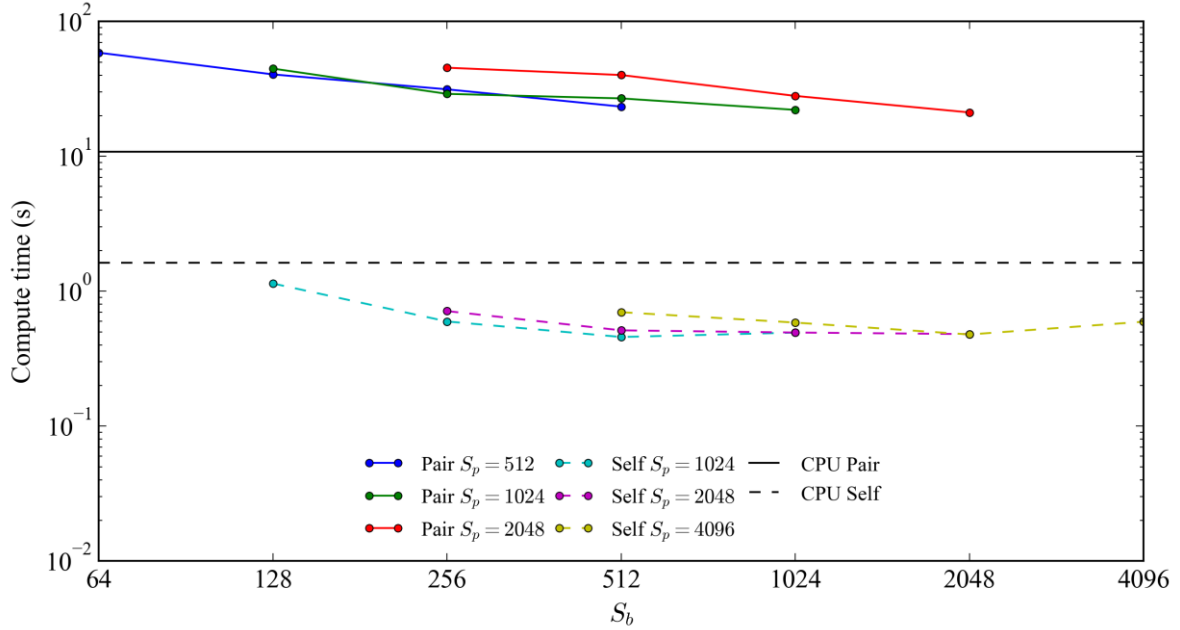


Figure 13. Variation of compute time on L40 GPU with  $S_p$  and  $S_b$  for  $N_p = 256^3$  using 32 host threads compared to CPU times with 32 threads.

Figure 14 shows profiling results for the density tasks which illustrate that data transfer and compute concurrency is minimal even for the more compute intensive self task types. This is an issue which is usually alleviated by keeping the SPH particle data on the GPU for the duration of the simulation but with task parallel solvers such as SWIFT this is not

possible since the tasks assigned to each thread are randomly generated by the scheduler in order to minimise thread idle time on the CPU. As such, a cell's density tasks may be assigned to one thread whilst it's force and gradient tasks may be assigned to another thread or stolen from the thread's queue by another thread.

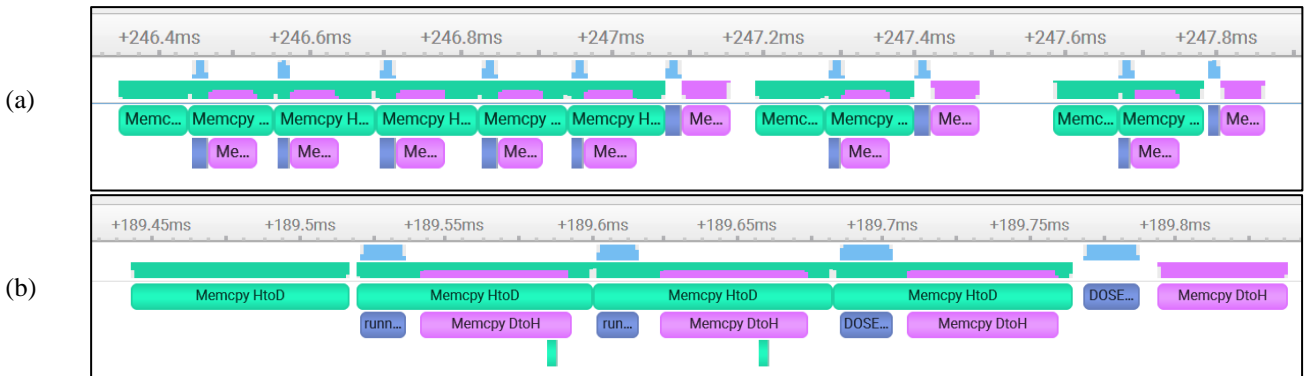


Figure 14. (a) Pair tasks with  $S_p=1024$  and  $S_b=512$ . Memcpys to the GPU and CPU are coloured green and pink respectively. Computation kernels are coloured blue. (b) Combination of self and pair tasks scheduled for execution on the GPU by two different host threads.

Figure 14 shows that although concurrency is achieved between data transfers to and from the GPU for these tests, concurrency with computations is minimal due to their relatively short duration which is why the GPU accelerated solver performs poorly on this machine.

### 3.4 Acceleration on Nvidia Grace-Hopper superchip

For this set of tests, the Grace-Hopper superchip nodes on the N8CIR Bede cluster are used to perform

the computations. The Grace-Hopper (GH200) consists of Grace (a 72 core ARM CPU) connected to Hopper (an H100 GPU) via specialised NVLink fabric capable of 450 GB/s (in each direction).

For the GH200 tests  $N_p=256^3$  particles and  $S_p$  was varied from 512 to 2048 for the pair tasks and 1024 to 4096 for the self tasks.  $S_b$  was also varied with four values used for each  $S_p$  to assess GPU offload efficiency. Figure 15 shows the compute times when tasks were executed on the H100 GPU with 32 host threads as compared to task execution on 32 threads

of the Grace CPU. 32 threads were used to ensure consistency and comparability with all other analyses presented in Section 3.2.

The Grace CPU is roughly 2.75 and 2.54 times faster in executing the pair and self tasks, respectively, than the POWER9 CPU whilst the best performing case executed on the H100 GPU for pair and self tasks is 2.05 and 2.06 times, respectively, faster than the V100 (Figure 6). The maximum speedups achieved when computing tasks on the H100 vs 32 threads of the Grace CPU are roughly 2.3 and 8.8 which are similar to the V100 tests *as compared to the POWER9 CPU*. When not including the packing and unpacking times the H100 GPU speedups are 6.6 and

23.8 when compared to 32 threads on the Grace CPU. The patterns followed by the GPU offload efficiency with variation of  $S_p$  and  $S_b$  are very similar to the patterns observed with the V100-POWER9 combination discussed in Section 3.2. This is expected as the architecture is similar due to the use of NVLink instead of PCIe to connect the CPU to the GPU. Analysing the overall time required to offload to the GPU for the best performing test with  $S_p=4096$  and  $S_b=1024$  and  $S_p=2048$  and  $S_b=512$  for the self and pair task types, respectively, the ratio of packing and unpacking time in comparison to the total offload time was approximately 65% further highlighting the importance of optimising the packing and unpacking process.

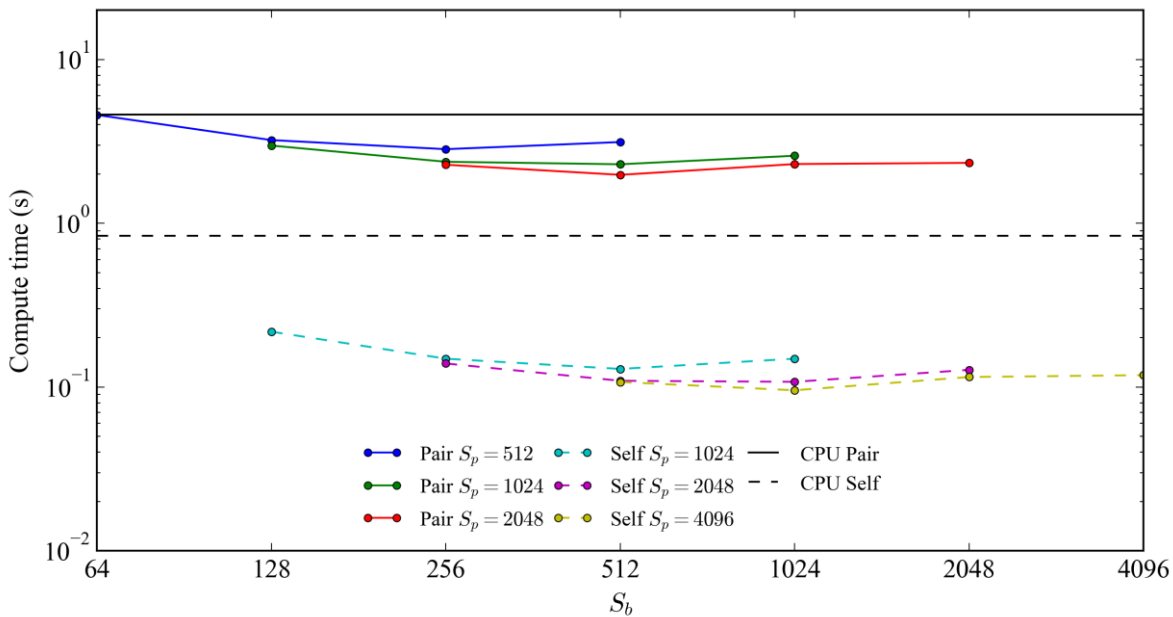


Figure 15. Variation of compute time on GH200 with  $S_p$  and  $S_b$  for  $N_p = 256^3$  using 32 host threads compared to CPU times with 32 threads.

The SWIFT CPU solver test was repeated to use the full Grace CPU with 72 threads in order to compare the full Grace CPU with the Hopper GPU. The full CPU (72 threads) was able to complete the self and pair tasks in 0.374 s and 2.09 s, respectively, in comparison to 0.838 and 4.61 s for 32 CPU cores. This is a near linear speedup, 2.24 and 2.21 times faster. The speedups for the GPU accelerated code executed on a Hopper GPU in comparison to execution a full Grace CPU using 72 cores are 1.04 and 3.93 for the pair and self tasks, respectively. Whilst the speedups for the self tasks are promising, the pair tasks are not accelerated by GPU execution and this is due to the pair tasks requiring larger data transfers to the GPU whilst performing less computations than the self tasks. Since the CPU already has the data to hand and also uses the highly efficient pseudo-Verlet list (Gonnet et al., 2013) discussed in Section 2.2.2 for the pair tasks, which

are not implemented in the GPU computations, the current implementation is unable to provide a significant speedup for the pair tasks.

### 3.5 Summary of analyses

The results of the analyses in Section 3 are summarised in Table 3 below where the best performing cases are presented. Table 3 shows that the H100 and V100 GPUs connected via proprietary connections perform significantly better than the L40 GPU connected to the CPU via PCIe. Table 3 also shows that for the best performing GPUs the packing/unpacking process is a significant portion of the GPU offload process.

Table 3. Hardware performance summary. All CPU results are using 32 threads for consistency. The speedups presented are based on the time required to compute all the SPH task types (self and pair) and subtypes (density, gradient and force) offloaded to the GPU.

Hardware	Total time (self and pair tasks)	Packing and Unpacking time	Best combination of $S_p$ and $S_b$	Speedup with packing	Speedup without packing
2 POWER9 CPU (32 cores)	14.8 s	0 s	NA	1	1
Nvidia V100 GPU	4.27 s	1.99 s	$S_p=2048, S_b=512$	3.47	6.49
Grace CPU (72 cores)	5.45 s	0 s	NA	1	1
Nvidia H100 GPU	2.07 s	1.34 s	$S_p=4096, S_b=1024$	2.63	7.47
2 Intel Xeon Gold 6330 CPU (28 cores)	12.5 s	0 s	NA	1	1
Nvidia L40 GPU	23.8 s	5.17 s	$S_p=1024, S_b=512$	0.52	0.67

## 4 SOLVER PERFORMANCE FOR A FULL SIMULATION

For the analyses presented in Section 3, the focus was on assessing the performance and potential of GPU acceleration of SWIFT’s SPH tasks. In this Section, a higher level analysis is presented focussing on overall performance on the Grace-Hopper superchip for a full simulation where non-SPH task types are executed on the CPU and where the overheads of task management are also assessed.

### 4.1 Original SWIFT CPU code performance:

The Gresho-Chan Vortex simulation, presented in Section 3, is used with  $N_p=256^3$  particles for the analyses presented here.

The unmodified SWIFT CPU code provides a 32-CPU thread base-line for comparison with the GPU accelerated code. Figure 16 (a) shows the analysis for a representative time step illustrating when each task is executed and by which CPU thread. At the start of the step, there is a small gap of roughly 52 ms which is when CPU threads are organising and activating the SPH interaction and time integration tasks required for the time step. The initial task management time is approximately 1.5% of the total time required to complete the step (4410 ms). For this case the initial conditions are setup such that the domain is decomposed into  $16^3$  top-level cells which may then be split into as many cells as the SWIFT solver deems necessary to achieve adequate fine-graining whilst minimising task management overheads. Analysis of the level at which tasks are finally created showed that most tasks were created as sub-self and sub-pair tasks rather than self and pair tasks (discussed in Section 2.2.2) with approximately 4096 particles contained in each cell.

Whilst some pair tasks are created to compute interactions with  $\sim 64$  particles in each cell (16384 pair tasks for each task subtype), the majority of SPH computations are performed as either sub-self (4096 tasks) or sub-pair (36864 tasks). The task recursion method, as discussed in Section 2.2.2, is used to perform the SPH computations such that each particle in any task type only searches for neighbours within the ideal cell size which for this case would contain  $\sim 64$  particles.

To provide a performance comparison of the full Grace CPU to the Hopper GPU, the test is repeated but this time using all of the Grace CPU’s 72 cores. Figure 16 (b) shows the results where the full Grace CPU completes the time step in 2065 ms in comparison to 4410 ms when only using 32 CPU threads (Figure 16 (a)). The speedup from 32 to 72 threads of 2.13 is near perfect (the best achievable with perfect scaling would have been 2.25). The sum of each thread’s wall clock time required to complete all the SPH tasks (density, force and gradient task subtypes) was recorded as 136496 ms and 137641 ms for the tests with 32 and 72 CPU threads, respectively which translates to 4266 ms and 1912 ms when averaged over the number of threads to estimate the time-to-solution for the SPH tasks. The initial task management time for the 72 thread test was 79 ms on average which is less than 4% of the total time step. The number of particles updated through a full time step per second per CPU core may be used to provide a reference for comparison with other solvers. For the cases outlined above this was  $\sim 120k$  particles marched through one time step per second per core.

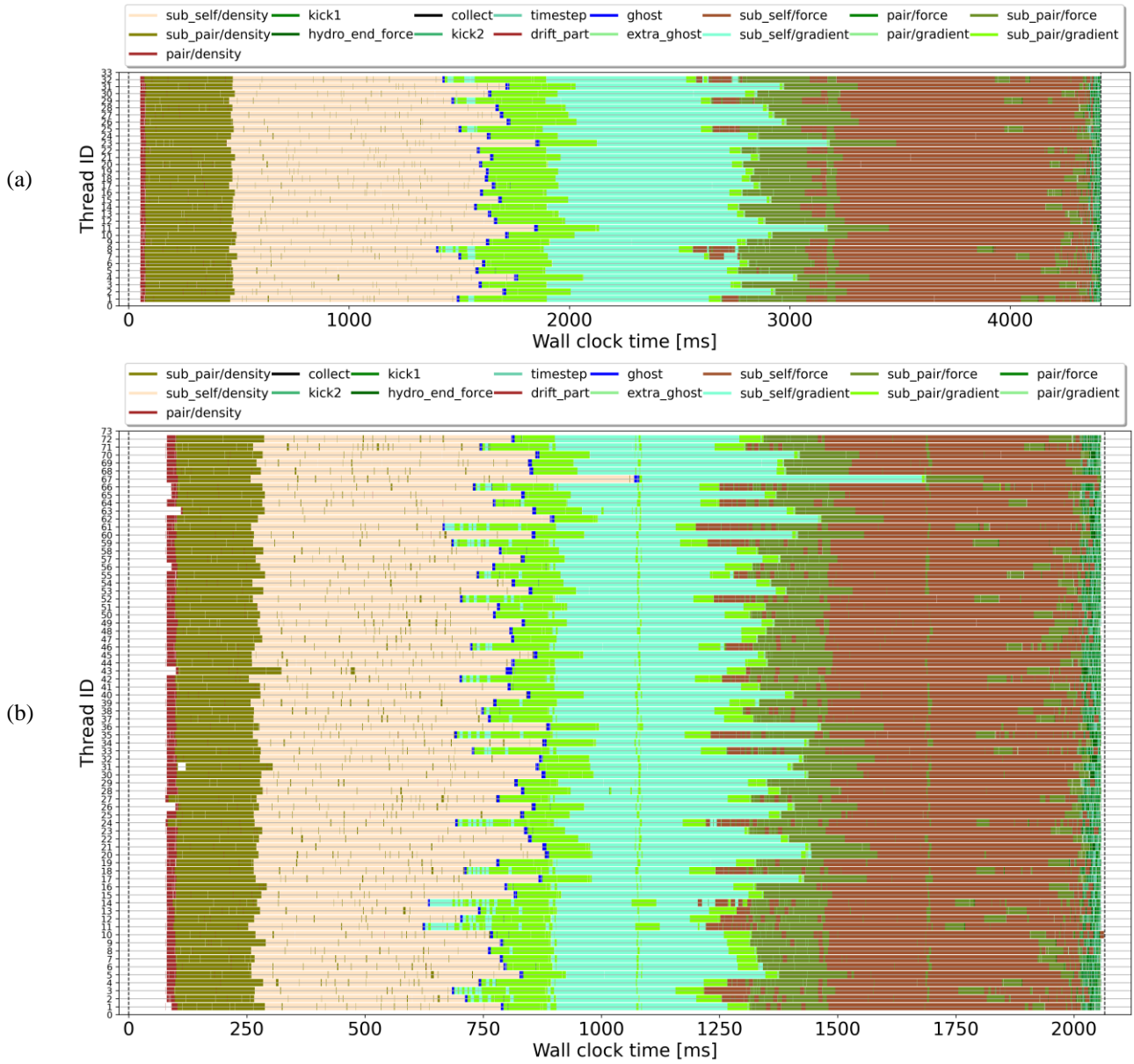


Figure 16. Tasks performed in a time step by the unadulterated SWIFT CPU code on the Grace ARM CPU. (a) Performance of 32 CPU threads. (b) Performance of 72 CPU threads. Each row illustrates which task type each CPU thread is executing at that point in time

## 4.2 GPU accelerated code performance:

The test in Section 4.1 is repeated using the GPU accelerated solver with 32 host CPU threads and the task execution is recorded for a representative time step. Figure 17 shows that the initial task management time is much greater for the GPU accelerated simulation where it is 388 ms in comparison to 52 ms (approx. 8x greater) when using 32 CPU threads to run SWIFT’s original CPU solver. Since the GPU solver is not currently able to perform the task recursion, as enabled for the CPU tests in Section 4.1, tasks are created at one level lower in the cell tree than the CPU solver tests. The choice of using cells containing  $\sim 512$  particles rather than the ideal size for GPU code efficiency (containing  $\sim 64$  particles) was made to minimise task management

overheads whilst only incurring minimal losses in efficiency due to the GPU code performing particle interactions using cells of width  $4h$  instead of  $2h$ . Using cells of size  $4h$  increases the number of “misses” in the computational loops where a particle searches for neighbours as each particle searches for neighbours in  $\sim 512$  particles instead of  $\sim 64$ . Increasing the cell size for the GPU tasks to a width of  $8h$  would minimise the initial task management time to be similar to the CPU tests however this would create more misses in the GPU particle interaction loops as each particle would search through 64 times more particles than required and only  $\sim 1.5\%$  of the neighbours searched would fall within  $2h$ . To ensure the number of particles offloaded is similar to the number of particles for the

better performing combinations of  $S_p$  and  $S_b$  for the tests presented in Section 3.4 the values used here

were  $S_p=256$  and  $S_b=64$  for self task types (halved for pair task types).

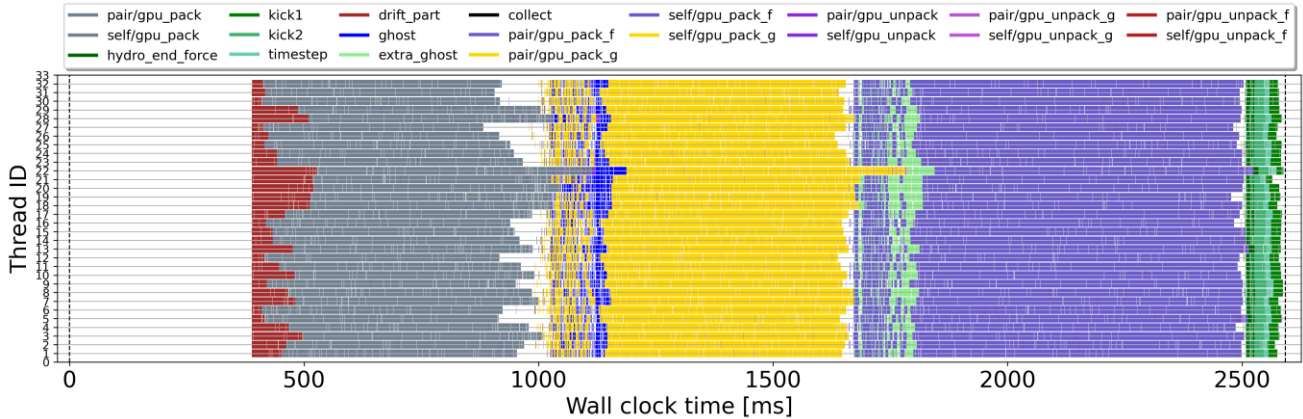


Figure 17. Tasks performed in a time step by the GPU accelerated SWIFT code. (a) Each row illustrates which task type each CPU thread is executing at that point in time. Tasks labelled `gpu_pack` are the pack tasks for the density task subtype where the data required for the GPU computations is packed into `part_send` arrays before offloading to the GPU once  $S_p$  tasks are packed. `gpu_pack_g` and `gpu_pack_f` are the pack tasks for the gradient and force task subtypes, respectively. Tasks labelled `gpu_unpack` are implicit tasks which serve to ensure the tasks depending on `gpu_pack` task subtypes are only unlocked after  $S_p$  `gpu_pack` tasks are completed. The dashed vertical line at the right hand side of the figure is the end of the time step.

The total time required to complete the time step with the GPU accelerated code was 2590 ms and the time required to complete all the SPH tasks was recorded as 57287 ms (1790 ms) when averaged over the number of host threads (32). In addition to the longer time spent managing tasks at the start of the simulation, there is notable idle time in-between task types as shown in Figure 17 especially towards the end of the density tasks (coloured grey and labelled as `self/gpu_pack` and `pair/gpu_pack`). The total time where threads were not executing computational tasks was 18107 ms (~566 ms when averaged over 32 threads) as compared to the full Grace CPU results (6838 ms or ~95 ms when averaged over 72 threads). It is currently unclear exactly what is causing this idle time in-between tasks but what is clear is that some threads are unable to retrieve tasks from their queues. Since tasks are offloaded to the

GPU in packs of  $S_p$  tasks, the tasks dependent on these  $S_p$  tasks must wait until the task results are copied back onto the CPU memory before they are unlocked and then enqueued as illustrated in Figure 5. This leaves some queues empty as they wait for tasks to be unlocked. The GPU performance is still an improvement (a speedup of 1.07) in comparison to the thread averaged time required for the Grace CPU to complete the SPH tasks with 72 threads using the original highly optimised SWIFT solver, 1912 ms. This speedup is similar to the speedup presented in Section 3.4 for the pair tasks (1.04) and is expected since SWIFT’s computations are dominated by pair tasks of which there are 13 times more than there are self tasks, further development is required in order to achieve our target of  $O(10)$  or greater speedups and this is discussed in Section 4.4.

### 4.3 Summary of analyses:

The results of the analyses in Section 4 are summarised in Table 4 below.

Table 4. Summary of CPU and GPU code performance for a full simulation

Hardware	Total step time	Initial task management time	Total time spent outside task execution	Time spent executing all density, gradient and force task subtypes	Total number of tasks
Nvidia Grace CPU (32 threads)	4.41 s	52 ms	63 ms	4.27 s	233,472
Nvidia Grace CPU (72 threads)	2.06 s	79 ms	95 ms	1.91 s	233,472
Nvidia H100 GPU	2.59 s	388 ms	565 ms	1.79 s	1,448,064

## 4.4 Limitations:

### 4.4.1 Packing/unpacking

In the current SWIFT SPH solver the data structures used to access and store the particle data are too complex to be efficiently copied across to the GPU, without re-organising them into simpler data structures first, and this has been a major factor limiting the achievable speedups. As discussed in Section 3.4, when the CPU-GPU data transfers and the GPU computation kernels are at their most efficient, the packing and unpacking process becomes a major bottleneck taking up to 65% of the total time required to prepare and offload the computations to the GPU.

### 4.4.2 High ratio of communications to computations for pair tasks

For self tasks, most particles in a cell are within  $2h$  of each other and therefore the ratio of communications to computations is relatively low which is why the GPU code can achieve good speedups. For pair tasks however, most particles involved are  $>2h$  away from each other especially when the two cells involved in a pair task are connected by an edge or a vertex. With the current approach all the task data for pair tasks must be sent to the GPU where the code loops through the particles to find their neighbours and perform the necessary computations. In the CPU code, the data is already in memory which minimises the overhead of data transfer. Pair tasks are also highly optimised on the CPU where a pre-sorting procedure is used to identify potential neighbours *a priori* to looping over them which minimises missed iterations in the loops over neighbouring particles (most particles looped over will be within  $2h$  when using the pre-sorting procedure). This optimisation could prove highly beneficial if applied to the GPU code as the ratio of communications to computations would be minimised greatly improving efficiency.

### 4.4.3 Task management overheads

Another major limitation of the GPU accelerated solver arises from the fact that in order to achieve highly optimised GPU computations, each individual task executed by the GPU was designed to act over particles in a cell with width  $2h$ . Whilst packing tasks into large bundles of  $O(100)$  tasks to be executed concurrently by the GPU (as discussed in Section 2.3.2) overcomes limitations associated with GPU instruction overheads (CPU-GPU copies and kernel launches). This gives rise to excessively fine-grained tasks and creates even greater overheads associated with managing  $O(100)$  times more tasks in comparison to the original SWIFT

CPU code. Increasing the cell size for GPU tasks to include 8 times the number of particles minimises task management overheads to an extent but decreases the efficiency of the GPU computations as  $>7/8$  of the computations are misses where particles are at a distance greater than  $2h$  from each other. Increasing the cell size also increases the ratio of data transfer to GPU computations which is also detrimental to GPU performance.

### 4.4.4 Adaptive resolution

The current task management scheme for the GPU code does not take into account cases with large disparities in smoothing length between particles and as such is not optimised for such cases. This prevents efficient computations involving gravity where some particles are drawn to each other, clustering and compressing with their smoothing length decreasing drastically, whilst other particles remain dispersed in nearby regions. In the CPU SWIFT solver, large variations in smoothing length are managed via task recursion, discussed in Section 2.2.2, which is designed to recurse through parent tasks creating tasks in deeper levels of the tree until the interaction of particles in neighbouring cells is optimised. This task recursion is not implemented for the GPU solver and as such the code is currently unable to efficiently handle cases with large variations in particle smoothing lengths.

## 5 CONCLUSIONS AND OUTLOOK

In this paper, a novel method for GPU acceleration within task-parallel solvers has been presented. The method performs well for accelerating the task computations on hardware designed for heterogeneous computing with state-of-the-art CPU-GPU connections achieving 2.6 to 3.5 times speedup when only comparing the time required to execute tasks acting on particles in cells with width  $\approx 2h$  on the GPU to 32 CPU threads. However, on hardware using conventional PCIe connections between the CPU and GPU the task computations are not accelerated (the achieved speedup was 0.52 in comparison to 32 CPU cores) as the CPU-GPU data transfers become the bottleneck. With the proposed approach as implemented in SWIFT, data re-arrangement and packing is required to allow for efficient data transfers and computations however this currently takes 65% of total offload time for the best performing cases. Optimising the packing process, or eliminating it altogether by re-structuring the data used in the CPU code to match the form optimised for the GPU, could double the achieved speedups.

For the approach proposed in this paper, where the task scheduler operations and other highly memory-bound tasks are left for the CPU whilst the GPU handles more computationally intensive tasks, it is clear that CPU-GPU superchips are a necessity. This is because the super-fast CPU-GPU connections in these superchips minimise latency and bandwidth bottlenecks of data transfers between the CPU and GPU. Given the demonstrated benefits of superchips for heterogeneous computing, when compared to traditional PCIe connected GPUs, it is anticipated that superchips will become mainstream in HPC as most scientific HPC applications require a mixture of low intensity and high intensity computations, not all of which would benefit from GPU acceleration as compared to execution on CPUs.

Performance over a full simulation was also assessed where it was evident that the solver was functioning in a truly heterogeneous manner with CPU computations overlapping with GPU computations. However, the GPU accelerated solver was found to suffer from excessive task management overheads. This is due to the GPU code being designed to perform computations for tasks where each cell contains the ideal number of neighbours for SPH particle interactions in comparison to the CPU SWIFT code where larger tasks are created and the CPU recurses through pre-defined daughter cells for this large task such that the particle interactions are performed at the ideal level of the cell tree where the cell size is proportional to the search radius  $2h$  for the largest particle in that cell (discussed in Section 2.2.2). Still, even with the excessive task management overheads the GPU accelerated solver provided a 1.7 times speedup in comparison to 32 CPU threads and 0.8 times speedup in comparison to 72 threads of Nvidia's Grace CPU for computation of a time step.

The path towards overcoming the task management limitation and the idle time in-between tasks in Section 4.4.3 is clear and requires adapting the GPU code such that the code is able to recurse through parent cells in sub-tasks. This development is also crucial to addressing the limitations related to adaptive resolution discussed in Section 4.4.4 which also requires task recursion. Task recursion within the GPU solver will also greatly improve the initial task management time associated with creating tasks at too deep a level in the tree which leads to  $O(100)$  times more tasks than the number of tasks created by the CPU solver.

Schaller *et al.* (Schaller et al., 2024) have shown that SWIFT scales extremely well up to tens of thousands

of cores demonstrating that the implemented MPI communications algorithms are highly efficient. The GPU off-loading approach presented in this paper does not add any further communications aside from the CPU-GPU communications, which are captured in the timings results presented in Sections 3 and 4. The domain decomposition system is also unaltered from the original CPU version. Therefore, the GPU off-loading approach presented in this paper should scale similarly well when compared with the original CPU only version for tests conducted over multiple compute nodes with multiple GPUs each and offers a natural way of performing computations on thousands of GPUs connected via MPI.

## 6 ACKNOWLEDGEMENTS

The authors would like to thank EPSRC for funding the Particles At eXascale on High-Performance Computing (PAX-HPC) project with grant EP/W026775/1 in which the solver presented in this paper was developed.

This work made use of the facilities of the N8 Centre of Excellence in Computationally Intensive Research (N8 CIR) provided and funded by the N8 research partnership and EPSRC (Grant No. EP/T022167/1). The Centre is co-ordinated by the Universities of Durham, Manchester and York.

The authors acknowledge the use of resources provided by the Isambard-AI National AI Research Resource (AIRR). Isambard-AI is operated by the University of Bristol and is funded by the UK Government's Department for Science, Innovation and Technology (DSIT) via UK Research and Innovation; and the Science and Technology Facilities Council [ST/AIRR/I-A-I/1023].

The authors are also grateful to Alastair Basden whom facilitated access to Durham's hardware testbeds which were extremely useful for code development and testing and for numerous discussions which helped in crystallising some of the methods presented in this paper. The authors would like to thank Lee Margetts for facilitating access to the Gemini 2 machine at the University of Manchester. We also thank Peter Draper whose inputs and insights were extremely helpful for developing compilation scripts for the GPU accelerated solver. We also thank Mark Wilkinson for arranging access to Isambard-AI. We are grateful to acknowledge very helpful discussions with colleagues in the wider PAX-HPC project namely Phil Hasnip, Tobias Weinzierl and Mladen Ivkovic. Finally, we are grateful for the late Richard Bower

who was instrumental in developing the research project and securing funding for the research.

## DATA AVAILABILITY STATEMENT

The datasets in this article were derived from a publicly available code repository accessible via:

<https://github.com/abouzier-nasar/SWIFT>

The datasets will be shared on reasonable request to the corresponding author.

## REFERENCES

- Andrade, T., Salo, L. A., Aurrekoetxea, J. C., Bamber, J., Clough, K., Croft, R., De Jong, E., Drew, A., Duran, A. & Ferreira, P. G. 2022. GRChombo: An adaptable numerical relativity code for fundamental physics. *arXiv preprint arXiv:2201.03458*.
- Antoniadis, A. F., Drikakis, D., Farmakis, P. S., Fu, L., Kokkinakis, I., Nogueira, X., Silva, P. A., Skote, M., Titarev, V. & Tsoutsanis, P. 2022. UCNS3D: An open-source high-order finite-volume unstructured CFD solver. *Computer Physics Communications*, 279, 108453.
- Atchley, S., Zimmer, C., Lange, J., Bernholdt, D., Melesse Vergara, V., Beck, T., Brim, M., Budiardja, R., Chandrasekaran, S. & Eisenbach, M. Frontier: exploring exascale. Proceedings of the International Conference for High Performance Computing, Networking, Storage and Analysis, 2023. 1-16.
- Bilotta, G., Hérault, A., Cappello, A., Ganci, G. & Del Negro, C. 2016. GPUSPH: a Smoothed Particle Hydrodynamics model for the thermal and rheological evolution of lava flows. *Geological Society, London, Special Publications*, 426, 387-408.
- Borrow, J., Bower, R. G., Draper, P. W., Gonnet, P. & Schaller, M. 2018. SWIFT: Maintaining weak-scalability with a dynamic range of  $10^4$  in time-step size to harness extreme adaptivity. *arXiv preprint arXiv:1807.01341*.
- Borrow, J., Schaller, M., Bower, R. G. & Schaye, J. 2022. Sphenix: Smoothed Particle Hydrodynamics for the next generation of galaxy formation simulations. *Monthly Notices of the Royal Astronomical Society*, 511, 2367-2389.
- Cercos-Pita, J. L. 2015. AQUA<sub>gpusph</sub>, a new free 3D SPH solver accelerated with OpenCL. *Computer Physics Communications*, 192, 295-312.
- Chalk, A. & Bernard, G. 2017. *Task-based parallelism for general purpose graphics processing units and hybrid shared-distributed memory systems*. Durham University.
- Chang, P., Wadsley, J. & Quinn, T. R. 2017. A moving-mesh hydrodynamic solver for ChaNGa. *Monthly Notices of the Royal Astronomical Society*, 471, 3577-3589.
- Cook, S. 2012. *CUDA programming: a developer's guide to parallel computing with GPUs*, Newnes.
- Corporation, N. 2025. *CUDA C++ Programming Guide*. Nvidia Corporation.
- Crain, R. A. & Van De Voort, F. 2023. Hydrodynamical simulations of the galaxy population: enduring successes and outstanding challenges. *Annual Review of Astronomy and Astrophysics*, 61, 473-515.
- Cullen, L. & Dehnen, W. 2010. Inviscid smoothed particle hydrodynamics. *Monthly Notices of the Royal Astronomical Society*, 408, 669-683.
- David-Cléris, T., Laibe, G. & Lapeyre, Y. 2025. The shamrock code: I-smoothed particle hydrodynamics on GPUs. *Monthly Notices of the Royal Astronomical Society*, 539, 1-33.
- Deskos, G., Laizet, S. & Palacios, R. 2020. WInc3D: A novel framework for turbulence-resolving simulations of wind farm wake interactions. *Wind Energy*, 23, 779-794.
- Domínguez, J. M., Fournakos, G., Altomare, C., Canelas, R. B., Tafuni, A., García-Feal, O., Martínez-Estévez, I., Mokos, A., Vacondio, R. & Crespo, A. J. 2022. DualSPHysics: from fluid dynamics to multiphysics problems. *Computational Particle Mechanics*, 9, 867-895.
- Edwards, H. C., Trott, C. R. & Sunderland, D. 2014. Kokkos: Enabling manycore performance portability through polymorphic memory access patterns. *Journal of parallel and distributed computing*, 74, 3202-3216.
- Fusco, L., Khalilov, M., Chrapek, M., Chukkapalli, G., Schulthess, T. & Hoefler, T. 2024. Understanding Data Movement in Tightly Coupled Heterogeneous Systems: A Case Study with the Grace Hopper Superchip. *arXiv preprint arXiv:2408.11556*.
- Gonnet, P., Chalk, A. B. & Schaller, M. 2016. QuickSched: Task-based parallelism with dependencies and conflicts. *arXiv preprint arXiv:1601.05384*.
- Gonnet, P., Schaller, M., Theuns, T. & Chalk, A. B. 2013. Swift: Fast algorithms for multi-resolution sph on multi-core architectures. *arXiv preprint arXiv:1309.3783*.
- Gorobets, A. & Bakhvalov, P. 2022. Heterogeneous CPU+ GPU parallelization for high-accuracy scale-resolving simulations of compressible turbulent flows on hybrid supercomputers. *Computer Physics Communications*, 271, 108231.
- Gresho, P. M. & Chan, S. T. 1990. On the theory of semi-implicit projection methods for viscous incompressible flow and its implementation via a finite element method that also introduces a nearly consistent mass matrix. Part 2: Implementation. *International journal for numerical methods in fluids*, 11, 621-659.
- Guerrera, D., Cavelan, A., Cabezón, R. M., Imbert, D., Piccinali, J.-G., Mohammed, A., Mayer, L., Reed, D. & Ciorba, F. M. 2019. SPH-EXA: Enhancing the Scalability of SPH codes Via an Exascale-Ready SPH Mini-App. *arXiv preprint arXiv:1905.03344*.
- Guo, X., Rogers, B. D., Lind, S. & Stansby, P. K. 2018. New massively parallel scheme for incompressible smoothed particle hydrodynamics (ISPH) for highly nonlinear and distorted flow. *Computer Physics Communications*, 233, 16-28.
- Herten, A. Many cores, many models: GPU programming model vs. vendor compatibility overview. Proceedings of the SC'23 Workshops of the International Conference on High Performance Computing, Network, Storage, and Analysis, 2023. 1019-1026.
- Herten, A., Achilles, S., Alvarez, D., Badwaik, J., Behle, E., Bode, M., Breuer, T., Caviedes-Voullième, D., Cherti, M. & Dabah, A. 2024. Application-driven exascale: The

- JUPITER benchmark suite. *arXiv preprint arXiv:2408.17211*.
- Holmen, J. K., Sahasrabudhe, D. & Berzins, M. Porting Uintah to heterogeneous systems. Proceedings of the Platform for Advanced Scientific Computing Conference, 2022. 1-10.
- Hopkins, P. F. 2017. A new public release of the GIZMO code. *arXiv preprint arXiv:1712.01294*.
- Karnakov, P., Wermelinger, F., Chatzimanolakis, M., Litvinov, S. & Koumoutsakos, P. A high performance computing framework for multiphase, turbulent flows on structured grids. Proceedings of the Platform for Advanced Scientific Computing Conference, 2019. 1-9.
- Kegerreis, J., Eke, V., Gonnet, P., Korycansky, D., Massey, R., Schaller, M. & Teodoro, L. 2019. Planetary giant impacts: convergence of high-resolution simulations using efficient spherical initial conditions and swift. *Monthly Notices of the Royal Astronomical Society*, 487, 5029-5040.
- Kolla, H. & Chen, J. H. 2017. Turbulent combustion simulations with high-performance computing. *Modeling and Simulation of Turbulent Combustion*. Springer.
- Lindblad, D., Isler, J., Moragues, M., Sherwin, S. & Cantwell, C. 2023. Nektar++: Development of the Compressible Flow Solver for Large Scale Aeroacoustic Applications.
- López, J. M., Feldmann, D., Rampp, M., Vela-Martín, A., Shi, L. & Avila, M. 2020. nsCouette—A high-performance code for direct numerical simulations of turbulent Taylor–Couette flow. *SoftwareX*, 11, 100395.
- Mcintosh-Smith, S., Alam, S. R. & Woods, C. 2024. Isambard-AI: a leadership class supercomputer optimised specifically for Artificial Intelligence. *arXiv preprint arXiv:2410.11199*.
- Meng, Q. & Berzins, M. 2014. Scalable large-scale fluid–structure interaction solvers in the Uintah framework via hybrid task-based parallelism algorithms. *Concurrency and Computation: Practice and Experience*, 26, 1388-1407.
- Menon, H., Wesolowski, L., Zheng, G., Jetley, P., Kale, L., Quinn, T. & Governato, F. 2015. Adaptive techniques for clustered N-body cosmological simulations. *Computational Astrophysics and Cosmology*, 2, 1-16.
- Merzari, E., Coppo Leite, V., Fang, J., Shaver, D., Min, M., Kerkemeier, S., Fischer, P. & Tomboulides, A. 2024. Energy exascale computational fluid dynamics simulations with the spectral element method. *Journal of Fluids Engineering*, 146.
- Mignone, A., Zanni, C., Tzeferacos, P., Van Straalen, B., Colella, P. & Bodo, G. 2011. The PLUTO code for adaptive mesh computations in astrophysical fluid dynamics. *The Astrophysical Journal Supplement Series*, 198, 7.
- Morris, J. P. & Monaghan, J. J. 1997. A switch to reduce SPH viscosity. *Journal of Computational Physics*, 136, 41-50.
- Pabst, S., Koch, A. & Straßer, W. Fast and scalable CPU/GPU collision detection for rigid and deformable surfaces. Computer Graphics Forum, 2010. Wiley Online Library, 1605-1612.
- Pakmor, R., Springel, V., Coles, J. P., Guillet, T., Pfrommer, C., Bose, S., Barrera, M., Delgado, A. M., Ferlito, F. & Frenk, C. 2023. The MillenniumTNG Project: the hydrodynamical full physics simulation and a first look at its galaxy clusters. *Monthly Notices of the Royal Astronomical Society*, 524, 2539-2555.
- Pearson, C. 2023. Interconnect Bandwidth Heterogeneity on AMD MI250x and Infinity Fabric. *arXiv preprint arXiv:2302.14827*.
- Price, D. J. 2012. Smoothed particle hydrodynamics and magnetohydrodynamics. *Journal of Computational Physics*, 231, 759-794.
- Price, D. J., Wurster, J., Tricco, T. S., Nixon, C., Toupin, S., Pettitt, A., Chan, C., Mentiplay, D., Laibe, G. & Glover, S. 2018. Phantom: A smoothed particle hydrodynamics and magnetohydrodynamics code for astrophysics. *Publications of the Astronomical Society of Australia*, 35, e031.
- Ramachandran, P., Bhosale, A., Puri, K., Negi, P., Muta, A., Dinesh, A., Menon, D., Govind, R., Sanka, S. & Sebastian, A. S. 2021. PySPH: a Python-based framework for smoothed particle hydrodynamics. *ACM Transactions on Mathematical Software (TOMS)*, 47, 1-38.
- Sanz Lechuga, A. 2022. *Approaching the exascale simulation of subsonic turbulence with smoothed particle hydrodynamics*. Universitat Politècnica de Catalunya.
- Schaller, M., Borrow, J., Draper, P. W., Ivkovic, M., Mcalpine, S., Vandenbroucke, B., Bahé, Y., Chaikin, E., Chalk, A. B. & Chan, T. K. 2024. Swift: a modern highly parallel gravity and smoothed particle hydrodynamics solver for astrophysical and cosmological applications. *Monthly Notices of the Royal Astronomical Society*, 530, 2378-2419.
- Schaye, J., Kugel, R., Schaller, M., Helly, J. C., Braspenning, J., Elbers, W., McCarthy, I. G., Van Daalen, M. P., Vandenbroucke, B. & Frenk, C. S. 2023. The FLAMINGO project: cosmological hydrodynamical simulations for large-scale structure and galaxy cluster surveys. *Monthly Notices of the Royal Astronomical Society*, 526, 4978-5020.
- Schieffer, G., Wahlgren, J., Ren, J., Faj, J. & Peng, I. Harnessing integrated cpu-gpu system memory for hpc: a first look into grace hopper. Proceedings of the 53rd International Conference on Parallel Processing, 2024. 199-209.
- Sharma, A., Brazell, M. J., Vijayakumar, G., Ananthan, S., Cheung, L., Develder, N., Henry De Frahan, M. T., Matula, N., Mallowney, P. & Rood, J. 2024. ExaWind: Open-source CFD for hybrid-RANS/LES geometry-resolved wind turbine simulations in atmospheric flows. *Wind Energy*, 27, 225-257.
- Smith, A., Loh, G. H., Naffziger, S., Wu, J., Kalyanasundharam, N., Chapman, E., Swaminathan, R., Huang, T., Jung, W. & Kaganov, A. 2024. Interconnect Design for Heterogeneous Integration of Chiplets in the AMD Instinct™ MI300X Accelerator. *IEEE Micro*.
- Springel, V. 2005. The cosmological simulation code GADGET-2. *Monthly notices of the royal astronomical society*, 364, 1105-1134.

Springel, V. 2010. Moving-mesh hydrodynamics with the AREPO code. *Proceedings of the International Astronomical Union*, 6, 203-206.

Stone, J. M., Tomida, K., White, C. J. & Felker, K. G. 2020. The Athena++ adaptive mesh refinement framework: design and magnetohydrodynamic solvers. *The Astrophysical Journal Supplement Series*, 249, 4.

Teyssier, R. 2002. Cosmological hydrodynamics with adaptive mesh refinement-a new high resolution code called ramses. *Astronomy & Astrophysics*, 385, 337-364.

Vergara Larrea, V. G., Joubert, W., Brim, M. J., Budiardja, R. D., Maxwell, D., Ezell, M., Zimmer, C., Boehm, S., Elwasif, W. & Oral, S. Scaling the Summit: deploying the World's fastest supercomputer. High Performance Computing: ISC High Performance 2019 International Workshops, Frankfurt, Germany, June 16-20, 2019, Revised Selected Papers 34, 2019. Springer, 330-351.

Vogelsberger, M., Marinacci, F., Torrey, P. & Puchwein, E. 2020. Cosmological simulations of galaxy formation. *Nature Reviews Physics*, 2, 42-66.

Wadsley, J. W., Keller, B. W. & Quinn, T. R. 2017. Gasoline2: a modern smoothed particle hydrodynamics code. *Monthly Notices of the Royal Astronomical Society*, 471, 2357-2369.

Willis, J. S., Schaller, M., Gonnet, P., Bower, R. G. & Draper, P. W. 2018. An efficient SIMD implementation of pseudo-Verlet lists for neighbour interactions in particle-based codes. *Parallel Computing is Everywhere*. IOS Press.

Xu, Q., Jeon, H. & Annavaram, M. Graph processing on GPUs: Where are the bottlenecks? 2014 IEEE International Symposium on Workload Characterization (IISWC), 2014. IEEE, 140-149.

Zhang, C., Rezavand, M., Zhu, Y., Yu, Y., Wu, D., Zhang, W., Wang, J. & Hu, X. 2021. SPHinXsys: An open-source multi-physics and multi-resolution library based on smoothed particle hydrodynamics. *Computer Physics Communications*, 267, 108066.